



**Facultad
de
Ciencias**

**Caracterización de Aparatos de Carga Acoplada
(CCDs) con sistema de lectura skipper**

**Characterization of Charge Couple Devices (CCDs) with
skipper readout system**

**Trabajo de Fin de Grado
para acceder al
GRADO EN FÍSICA**

**Autora: María Pérez Martínez
Co-directora: Rocío Vilar Cortabitarte
Co-directora: Núria Castelló-Mor**

Junio 2023

Abstract

This final degree project comprehends the first commissioning of the IRONMAN setup, a CCD experimental setup established in a clean room at IFCA (Instituto de Física de Cantabria). The main components of this setup involve a vacuum chamber, a cryocooler and a CCD controller and readout system. Using this setup, a non-scientific Charge Couple Device (CCD) with skipper readout system, specifically the CCD P52-U model, has been characterized. Given the broad nature of CCD characterization, this study has focused on optimizing its configuration parameters to achieve the best single electron resolution and in the study of the influence of the temperature on the different manifestations of traps generated by the silicon defects.

During the characterization process, the effects of electromagnetic noise on CCD images resulted in an additional investigation of its impact on the images. The analysis of the influence of electromagnetic noise on the quality and readout noise of CCD PP52-U images has revealed the high sensitivity of the experimental setup to electromagnetic noise and has provided insights into various electromagnetic noise sources. Based on these findings, several ideas for improvement have been proposed to mitigate the influence of electromagnetic noise and enhance the overall quality and readout noise of the CCD images.

CCD configuration parameters have been satisfactorily optimized, resulting in an improvement of the charge collection, transfer, and readout processes. This optimization is essential for reducing and accurately calibrating the dark current, leading to more reliable estimations of the pixel readout noise.

Furthermore, the generation of traps by silicon defects and their impact on CCD images has been studied. These traps can manifest on the images in the form of bad columns, hot pixels, super hot pixels, and hot columns. As the temperature is raised, their progressive appearance has been observed and the changing behaviour of the hot columns has been specifically studied.

Keywords: CCD, configuration parameters, noise, skip images, non-skip images, dark current, silicon defects

Resumen

Este proyecto de fin de grado comprende la primera puesta en marcha del montaje experimental IRON-MAN, un montaje experimental de CCDs situado en una sala limpia en el IFCA (Instituto de Física de Cantabria). Los componentes principales de este montaje incluyen una cámara de vacío, un criocooler, y un controlador y sistema de lectura de CCDs. Utilizando este montaje, se ha caracterizado un Dispositivo de Carga Acoplada (CCD) no científico con sistema de lectura skipper, específicamente el modelo CCD P52-U. Dada el amplio campo que involucra la caracterización de las CCD, este estudio se ha centrado en la optimización de sus parámetros de configuración para lograr la mejor resolución de un solo electrón y en el estudio de la influencia de la temperatura en las diferentes manifestaciones de trampas generadas por los defectos de silicio.

Durante el proceso de caracterización, los efectos del ruido electromagnético en las imágenes de CCD dieron lugar a una investigación adicional de su impacto en las imágenes. El análisis de la influencia del ruido electromagnético en la calidad y el ruido de lectura de las imágenes de CCD P52-U ha revelado la alta sensibilidad del montaje experimental al ruido electromagnético y ha proporcionado información sobre varias fuentes de ruido electromagnético. Basándose en estos hallazgos, se han propuesto varias ideas de mejora para mitigar la influencia del ruido electromagnético y mejorar la calidad general y el ruido de lectura de las imágenes de la CCD.

Se ha optimizado de forma satisfactoria los parámetros de configuración de la CCD, lo que ha mejorado la eficiencia de los procesos de recopilación, transferencia y lectura de carga. Esta optimización es esencial para reducir y calibrar con precisión la corriente oscura, de tal forma que puedan obtenerse estimaciones más precisas del ruido de lectura de los píxeles.

Además, se ha estudiado la generación de trampas por defectos de silicio y su impacto en las imágenes de la CCD. Estas trampas pueden manifestarse en forma de columnas defectuosas, píxeles calientes, píxeles supercalientes y columnas calientes en las imágenes. A medida que se eleva la temperatura, se ha observado su aparición progresiva y se ha estudiado específicamente el comportamiento cambiante de las columnas calientes.

Contents

1	Introduction	1
1.1	Dark Matter and its direct detection	1
1.2	CCDs as Dark Matter detectors	1
1.2.1	DAMIC-M Experiment	2
1.3	Charge Coupled Devices (CCDs)	2
1.3.1	Skipper CCDs	8
1.3.2	Silicon defects in CCDs	12
1.4	Goals of this study	13
2	Experimental setup	14
2.1	Cryostat	14
2.2	Electronics	15
2.3	Detector	15
2.4	Remote control of operational parameters	17
2.4.1	Slow Control System	17
2.4.2	Data Acquisition (DAQ) machine	17
3	Study of non-electronic noise sources for the CCD PP52-U experimental setup	18
3.1	Non-skip images	18
3.2	Skip images	23
4	Optimization of CCD configuration parameters	30
4.1	Low voltage value of the summing well	32
4.2	High voltage value of horizontal clocks	33
4.3	Integration time	37
5	Study of silicon defects as a function of temperature	38
6	Conclusions	42
6.1	Future work	43
A	Analysis software	46
A.1	SAOImage DS9	46
A.2	WADERS	46
B	CCD configuration file	52
C	Guide to skipper CCD Start-Up and data-taking with the LEACH DAQ system:	
	CCDDrone	56
C.1	CCD Start-Up	56
C.2	Data-taking process	57
C.2.1	Scripts	58
D	Python codes	61
D.1	Integration time	61
D.2	Average FITS image	62

Chapter 1

Introduction

Discovering the nature of Dark Matter (DM) is expected to shed light on the origin of the universe, the development of galaxies, and the fundamental laws of physics. Its enigmatic nature offers an attractive invitation to push the limits of scientific investigation in an effort to answer one of the universe's most fascinating mysteries.

1.1 Dark Matter and its direct detection

The search for Dark Matter (DM) is a subject of extensive research in the fields of astrophysics, cosmology, and particle physics. There is strong astrophysical and cosmological evidence that supports the existence of this form of matter that accounts for around 27% of the universe's mass [1]. The hypothetical distribution of dark matter surrounding galaxies and other cosmic structures is referred to as dark matter halo. This concept arises from observations that indicate the presence of more mass within galaxies and galaxy clusters than can be accounted for by ordinary matter alone [2]. The solar system is within this halo, so it is believed that dark matter particles continuously pass through the Earth.

One of the most popular candidates for DM is known as Weakly Interacting Massive Particles (WIMPs). These particles are believed to have been in thermal equilibrium with radiation and baryon plasma in the early universe. As the universe expanded and cooled, the temperature dropped below the thermal level corresponding of WIMPs masses. Consequently, the number of WIMPs decreased to prevent annihilation. This phenomenon, known as freeze-out, resulted in a fixed number density of WIMPs. Thus, DM decoupled from the plasma, and its abundance remained fixed at the currently observed value.

Dark matter searches are conducted with three types of experiments: production at colliders, indirect detection and direct detection. DM does not emit, absorb, or interact with electromagnetic radiation, making it challenging to detect. Direct detection experiments have the purpose of identifying the low-energy nuclear or electron recoils that arise from the interactions between dark matter (DM) and ordinary matter. These subtle energy signals can be quantified via ionization, scintillation, and phonon measurements. There are numerous examples of these types of experiments [3], which are based in one or several technologies to measure these signals. Dark matter particles are believed to possess very weak interactions with ordinary matter, so these experiments require extremely low background noise to be able to distinguish potential signals from DM interactions. Therefore, direct detection experiments are typically located in deep underground laboratories in order to minimize the arrival of cosmic rays to the detectors [4]. Low radioactivity shielding and detector materials (including components associated to the detector such as electronics, wires, screws, etc.) are used to avoid environmental radiation produced in the vicinity of the detectors.

1.2 CCDs as Dark Matter detectors

Direct detection experiments such as DAMIC (DARk Matter In CCDs), DAMIC-M (DARk Matter In CCDs at Modane), Oscura or SENSEI aim to measure the ionization induced by DM by means of silicon

charge coupled devices (CCDs). The sensitivity of Si based detectors is limited by the dark current, inherent electronic noise, bulk and surface defects, and impurities in the Si crystal.

DAMIC (Dark Matter in CCDs) is specifically designed to detect low-mass dark matter particles, i.e. WIMPs, from small ionization signals induced by the scattering of DM particles with silicon nuclei inside the CCDs [5]. These signals need to be distinguished from background noise, reflecting the importance of high resolution for these devices. DAMIC is located at the SNOLAB underground laboratory at a depth of 2 km beneath a granite overburden and is shielded with radiopure materials to mitigate natural radioactivity and cosmic flux backgrounds [6]. DAMIC primarily conducted a measurement of WIMPs, along with calibrations, backgrounds, and electron scattering. In the initial phase (2017-2019), non-skipper CCDs were used to collect data. An excess of data was observed compared to the expected results in the measurement of WIMPs. To confirm or refute this excess, an improvement was made by employing two skipper CCDs. Recently published data [7], once again, shows an excess compatible with the previous findings, although the source of this excess is unknown. Several possibilities are being considered, ranging from a signal to the possibility of an unknown background in the CCDs themselves.

1.2.1 DAMIC-M Experiment

DAMIC-M (DAMIC at Modane) is the successor experiment of DAMIC at SNOLAB. This experiment will employ thick silicon charge-coupled devices (CCDs) to search for dark matter particles from the galactic halo of the Milky Way at the Laboratoire Souterrain de Modane (located at a depth of 1.7 km) in France. The leading innovation in DAMIC-M CCDs is the deployment of Skipper CCDs, i.e. CCDs with a novel skipper readout that achieves a single electron resolution level through multiple non-destructive charge measurements of the individual pixel charge. This optimized design helps to reduce the background noise and consequently to improve the sensitivity in detecting small ionization signals from nuclear and electronic recoils. Therefore, DAMIC-M will take a leap forward of several orders of magnitude in the exploration of the detection of nuclear and electronic recoils induced by dark matter particles [8].

DAMIC-M is currently in the development phase towards building a 200-massive (3.5 g), 9 Mpixel Skipper CCDs in an array to achieve a kg-scale target mass within an extremely low background environment at LSM. A prototype, the Low Background Chamber (LBC), with 20 g of low background Skipper CCDs, has been installed at the Laboratoire Souterrain de Modane since the end of 2021 and is currently taking data [9].

1.3 Charge Coupled Devices (CCDs)

CCDs are ionization collection devices formed by a two-dimensional grid of pixels identified by row and column indices. These devices have a variable number of read-out amplifiers, which are located at the ends of the outermost rows (serial registers). The amplifiers can be used individually or collectively to acquire images. These devices were originally invented in 1969 at Bell laboratories by Willard S. Boyle and George E. Smith, who received the 2010 Nobel Prize in Physics for their invention [10]. The original purpose for them was to work as memory storage units where the quantity that expressed a bit of information was the charge stored in each of the pixels. Currently these devices are being used as ionization imaging sensors due to their capacity to digitally image the interactions of incident radiation.

Each pixel behaves as a MOS (Metal Oxide Semiconductor) capacitor, which is composed of a polysilicon metal gate, an insulating layer of silicon dioxide and a silicon substrate, as it is shown in Figure 1.1. MOS capacitors used in CCDs have an n-channel design, meaning that the channel region is formed by a n-type substrate with a thin p-type layer buried beneath the silicon dioxide layer. The n-type substrate has a high resistivity so that the device can be fully depleted with a relatively low bias potential. This potential is applied to the backside contact of the CCD and generates an electric field that creates a depletion region, i.e. a region of the semiconductor substrate fully depleted of free charge carriers (electrons or holes). This region is the one where signal ionization charge is produced.

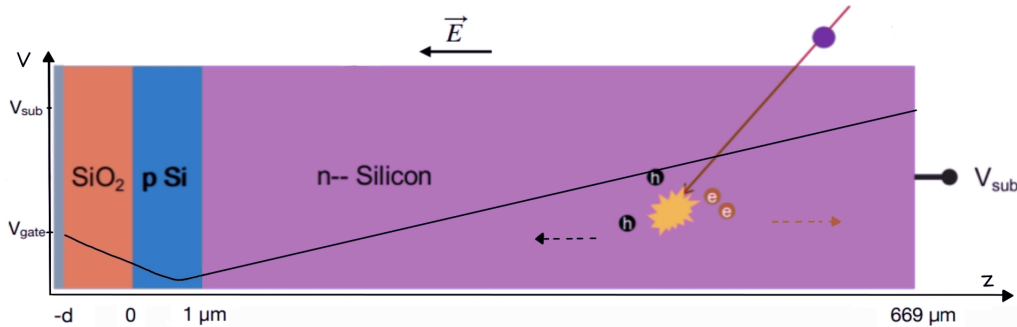


Figure 1.1: Cross-sectional diagram of a CCD pixel that shows its internal structure, the voltage along the different layers and the drift directions of electrons and holes under the influence of an electric field that fully depletes the device and that has been generated due to a bias voltage V_{sub} applied to the backside contact. The minimum potential is the point at which holes are collected. Picture from [11].

The operation of a CCD can be divided into three stages: detector exposure and charge collection, charge transfer, and charge readout.

During the exposure time if the energy of the incoming particles is greater than the band-gap of silicon, electron-hole pairs are created in a process called ionization. Holes are swept by the electric field towards the top gate structure and they are held in the buried channel until transfer begins. Electrons are drifted towards the backside contact where the bias voltage is applied. As the charge carriers drift, they also undergo lateral diffusion in both the x and y directions. This diffusion can potentially result in the collection of signal charges in a different pixel with respect to the region they were produced.

Once the exposure time ends, charge transfer begins pixel by pixel. Each pixel consists of three gate contacts (3-phase CCD) and by an appropriate sequencing of the gate voltages, which can be switched independently from low to high or vice versa, it is possible to transfer charge from one pixel to another across the CCD in a process known as *clocking*. In Figure 1.2 an example of clock sequencing is shown. The CCD array is schematically represented in Figure 1.3. The charge generated in the active region of the CCD can be clocked vertically upwards towards the serial register 2 (SR2), vertically downwards towards SR1, or simultaneously to both serial registers. Since channel stops are located between columns and all the pixels are connected to the same clock source, a single clock cycle transfers in the same vertical direction all pixels charge of each of the rows to the corresponding pixels of the following row. The last vertical clock moves charge from the active region into the serial register, and it happens across the Transfer Gate. Only when this gate is at its low potential value charge is transferred into the serial register. In this region charge is clocked horizontally towards side U (right side) or side L (left side) and at the end of both sides charge is moved into an external circuit for the readout process.

The reading of the charge accumulated in each pixel is crucial, since the technique used mainly defines

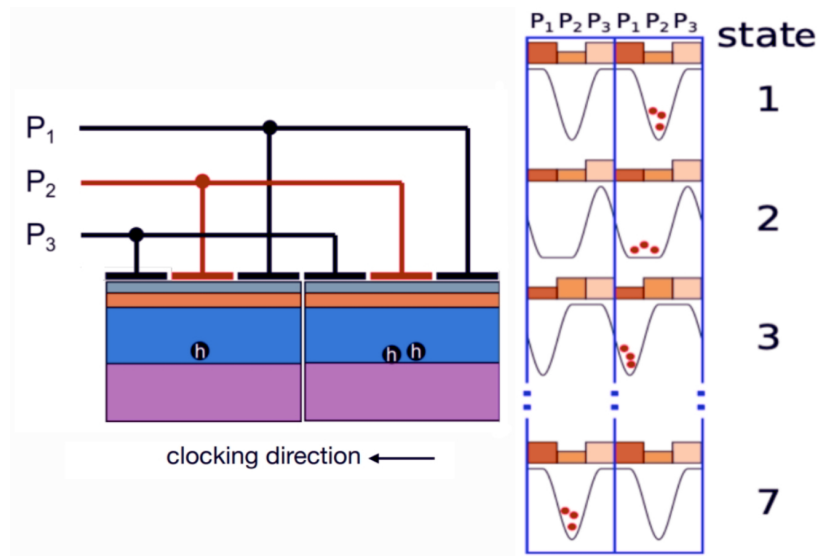


Figure 1.2: At the right it can be seen the clocking sequence for transferring charge from one pixel to another. Picture from [12]. At the left it is shown the 3-phase gate structure of two pixels, the right pixel corresponds to state 1 whereas the left pixel to state 7. Picture from [11].

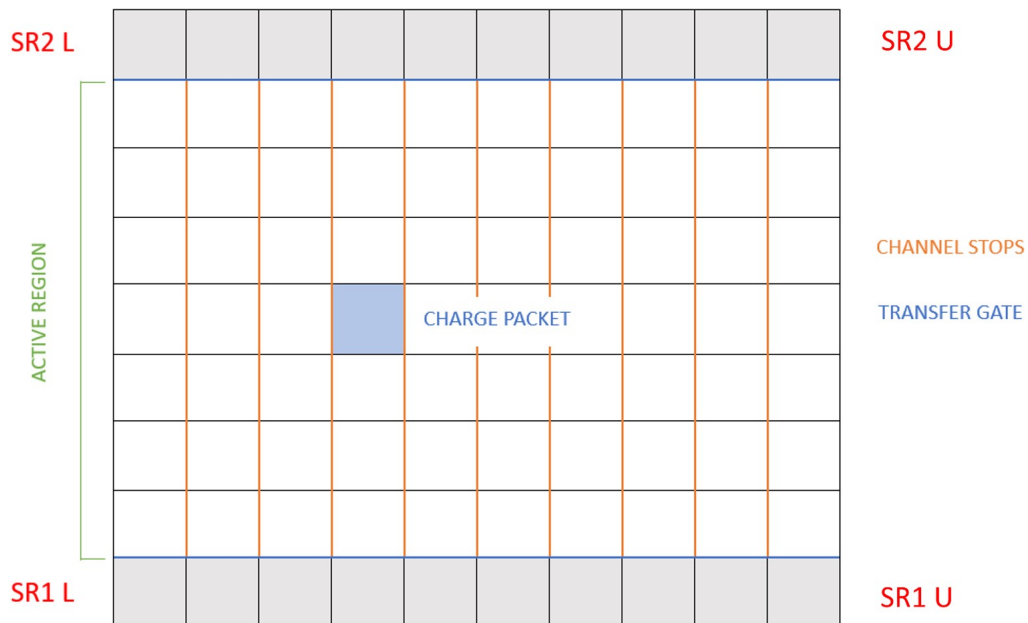


Figure 1.3: Schematic drawing of the active region and serial registers (SR) of the CCD with labeled features.

the CCD's image reading noise. CCD's readout stage includes multiple gates, as well as two transistors: the reset switch and the output amplifier. Figure 1.4 shows a circuit diagram for the readout amplifier.

After the charge exits the serial register, it goes through the Summing Well gate (SW) and the Output Gate (OG) before being dumped into the Sense Node (SN), a capacitor where pixel charge is measured. The charge transferred into the SN results in a change in the electrical potential of the node proportional to the charge magnitude, which is sensed by and passed through the output JFET and is further amplified. This amplified signal is the video signal sent out of the CCD, which will be digitized with a 16-bit Analog-to-Digital-Converter (ADC). Charge is cleared by means of a reset pulse that triggers

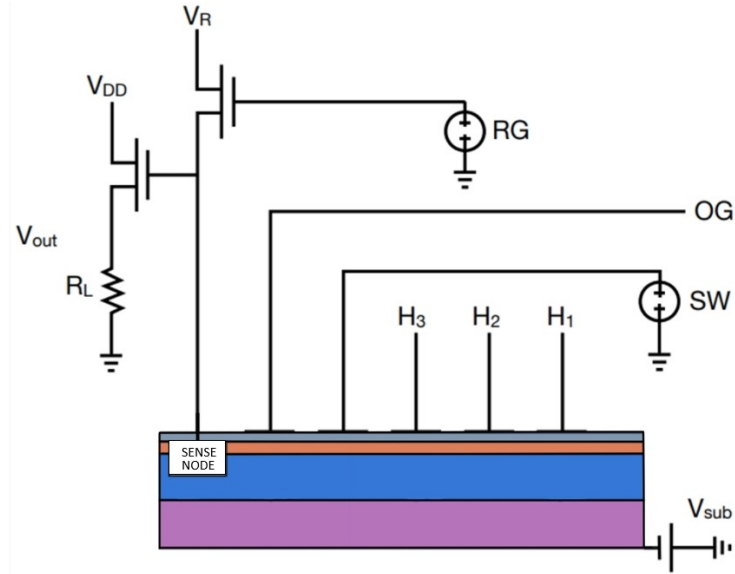


Figure 1.4: Circuit diagram of CCD readout. Picture from [4].

a discharge by the reference voltage V_R . A differential measurement of the charge is made before and after adding it into the Sense Node to prevent fluctuations in the SN potential measurement after the reset pulse is sent, i.e. to avoid measuring charge generated and injected into the SN every time the reset pulse is sent. To even reduce more the noise, the video signals in the differential measurement are integrated using a technique called Correlated Double Sampling (CDS). The differential measurement employing this technique consists on initially sending a reset pulse that triggers a discharge by V_R when the charge is in the SW. Immediately after, the integral of the sense node value is measured for an integration time¹ τ_{int} . This measurement is called the “pedestal level” and provides a reference level for charge measurement. Then, charge is clocked from the SW through the OG into the SN and the video signal is integrated again for τ_{int} , this value is called the “signal level”. In Figure 1.5 it is shown the video output trace with pedestal and signal measurements. After the signal measurement, the reset pulse is triggered to flush charge and the whole process is repeated until the serial register has been completely read out. The reading system obtains the charge level collected in a pixel as the difference between the signal level and the pedestal level. Doing this differential measurement employing the CDS technique guarantees a significantly improved charge calculation as any fluctuations caused by the reset pulse in the charge measurement of each pixel can be eliminated using this technique. CDS integration can effectively compensate for high frequency noise, essentially by the central limit theorem. However, it is not sufficiently effective enough in reducing low frequency noise, which remains in the CCD readout (see Figure 1.6).

As it has already been mentioned, the values measured for each pixel are digitized with a 16-bit Analog-to-Digital-Converter (ADC) and then sent over a fiber optic cable to a computer where the information is stored as a FITS (Flexible Image Transport System) file. Analog-to-digital units (ADUs) are 16-bit numbers proportional to the number of charge carriers collected in each pixel by way of the gain k (ADU per e^-). CCD images store a stacked record of all ionization signals produced during the exposure time in a two-dimensional format. If the CCD is clocked more rows in y or x than exist in the device one gets an image larger in x or y than the size of the detector. These extra pixels are referred to as overscans and the difference between vertical and horizontal overscans relies on the time exposure

¹The optimum value of the integration time is determined experimentally depending on how its value affects the noise of the system.

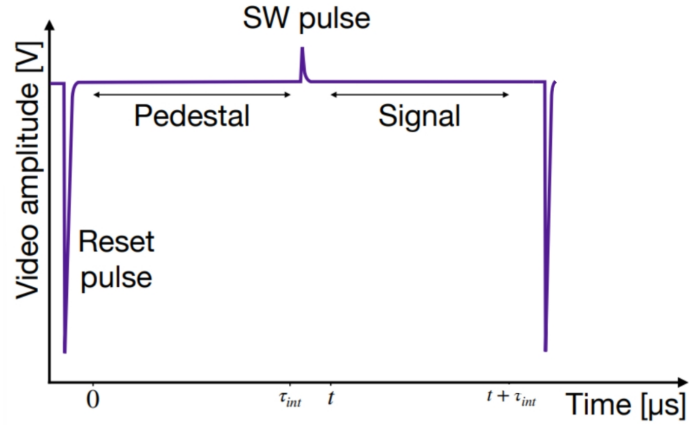


Figure 1.5: Conventional CCD video output trace. Figure from [4]. A reset pulse is sent and then the pedestal level is measured for an integration time τ_{int} . Afterwards the SW is triggered and charge is transferred to the SN, where the signal level is measured for τ_{int} . A reset pulse is sent again to clear the charge from the SN.

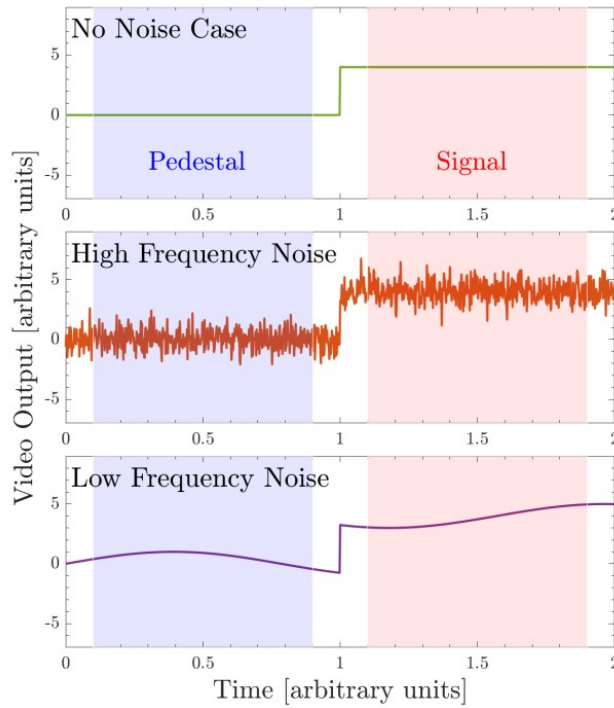


Figure 1.6: Comparison of performing the CDS technique in a differential charge measurement in a case without noise (top panel), a case with high frequency noise components (middle panel) and a case with low frequency noise components (bottom panel). Figure from [11]. CDS is effective for the high-frequency noise component but not for low-frequency noise.

of their pixels. Horizontal overscans (x-overscans) corresponds to reading the serial register past the length of a row. Since this process is extremely quickly the extra pixels will have almost no charge, so these pixels provide the baseline or pedestal of an image, i.e. the ADU value that corresponds to 0 charge in e^- units. However, vertical overscans (y-overscans) will contain charge accumulated proportional to the amount of time it takes to read the whole size of the CCD. Images are typically viewed using the SAOImageDS9 visualization tool (see the appendix section A.1). In Figure 1.7 a CCD image visualized with “DS9” is shown with the vertical and horizontal overscans being labelled. For this image, the pixels have been read one by one. However, it is possible to read out consecutive pixels.

This process is known as *binning*. For instance, if an image is binned 5×10 , the charge from 5 pixels is dropped together into the readout stage from the serial register (x-binning) while charge from 10 rows of pixels is vertically pushed together into the serial register before being clocked horizontally (y-binning).

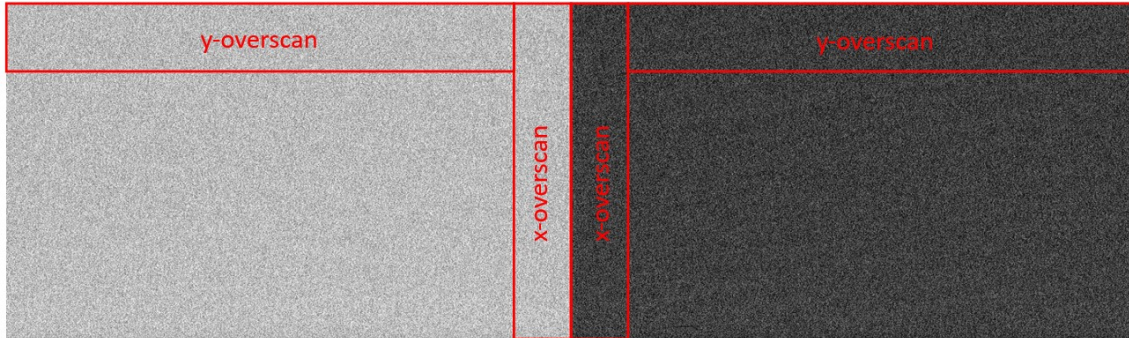


Figure 1.7: A non-skip image visualized with the “DS9” software. The left half side of the image has been taken with the left amplifier (L) while the right half side has been taken with the right amplifier (U). The x and y-overscans are labelled.

The baselines for the U and L amplifiers are different, as shown in Figure 1.7. However, this difference does not imply that one of the amplifiers has a higher charge, as the charge is only proportional to the pixel content after pedestal subtraction. This process is commonly referred to as equalization. The distribution of image pixel pedestal-subtracted values in ADUs or e^- is referred to as the *pixel charge distribution* (PCD). A background-free PCD, i.e. with no charge present in the pixels, should follow a Gaussian with mean 0 (after the equalization process the charge distribution of all pixels is centered at zero) and standard deviation equal to the readout noise of the device if the CCD is working correctly.

Since the CCD is operating in total darkness, it can be seen in the images ionization signals produced by alpha particles, electrons and muons. Each of these events produce a distinctive track which allows to differentiate them. There is another series of events referred to as point events that can be produced by X-rays, gamma rays or any other particle that deposits a low amount of energy such as neutrons, hopefully DM candidates, neutrinos or low energy electrons. Figure 1.8 depicts an image fraction of the CCD with all these ionization tracks labelled. The ionization of an alpha particle takes place in a small volume but due to the plasma effect the resulting charge is dispersed over multiple pixels, creating a thick dot on the image. The electron ionization process involves electron scattering with electrons and silicon nuclei, which results in a curved track. Since the muon mass is 207 times greater than the electron mass, it does not change its direction, leaving a straight track in the image [13]. It is possible to distinguish between the front and back of a muon track. The back of the track is characterized by a wider width, which is attributed to the charge carriers traveling a greater distance and consequently exhibiting greater diffusion.

After charge has reached the surface of the CCD, determining which pixels correspond to ionization tracks can be done by several algorithms. The clustering process makes it possible to distinguish and classify different particles from one another by finding groups of adjacent pixels that belong to different ionization tracks. Each of these tracks are referred to as clusters. The masking process involves selectively removing certain pixels, such as clusters corresponding to ionization tracks.

Dark current refers to charges generated in the device when no outside radiation is falling upon the detector; such as electron-holes pairs generated thermally, defects on the silicon crystalline structure, etc. These generated charges contribute to the readout noise as they are collected in pixels. Lowering

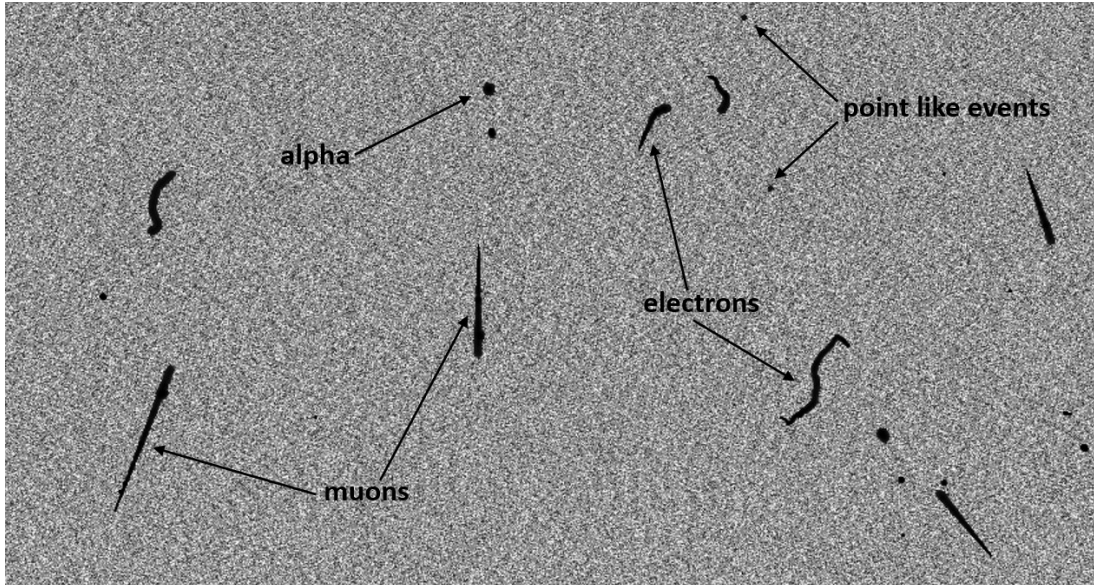


Figure 1.8: Image fraction visualized with “DS9” in which tracks produced by different types of particles are shown and labelled.

the detector temperature reduces the dark current, as the probability of electron-hole pair generation due to thermal effects follows the formula $T^{1.5} e^{\frac{E_g}{2k_B T}}$ [14]. This is the reason why DAMIC CCDs are operated at temperatures equal to or lower than 140 K. To only measure the dark current is important to effectively remove clusters corresponding to ionization tracks using the mentioned processes (clustering and masking processes). It is important to emphasize that these processes are not limited to only finding and removing clusters corresponding to ionization tracks.

1.3.1 Skipper CCDs

Skipper CCD technology was first proposed by Janesick et al. [15]. CCDs with the skipper readout system have an output structure that allows multiple measurements of the pixel charge, referred to as Non-Destructive Charge Measurements (NDCMs). Modelling pixel charge as the actual induced ionization with an additional Gaussian white noise component from readout and averaging over the N different measurements (skips) allows to reduce the noise by $\sigma_{pix} \rightarrow \sigma_{pix}/\sqrt{N}$. Figure 1.9 plots an example of skipper image resolution as a function of the number of skips. For a large number of skips, sub-electron noise levels are achieved. Skipper CCDs can overcome the low frequency noise component that limits standard CCDs by employing a shorter integration times to measure the pedestal and the signal levels, as shown in Figure 1.10. It is important to note that even though the skipper technology highly reduces noise, the time it takes to read the images is highly increased.

The distinction between conventional and skipper CCDs relies on the output stage structure. Skipper CCDs use floating gates whereas the conventional ones use floating diffusion gates. The term floating simply refers to the fact that the sense node is electrically isolated. The sense node is created by heavily p-doping the n-type substrate, which results in the formation of a diffusion region with high resistivity. A floating diffusion gate directly connects the highly doped diffusion region and the reset transistor as well as the MOSFET amplifier through an ohmic contact. [17]. The isolated diffusion region acts like a capacitor so that the pixel charge that reaches this region causes a voltage change V_c of the sense node. When the reset pulse is sent, the voltage is set back to V_R (reference voltage), which destructively flushes out the charge. Skipper CCDs use a floating gate as the readout node so that the SN can operate as

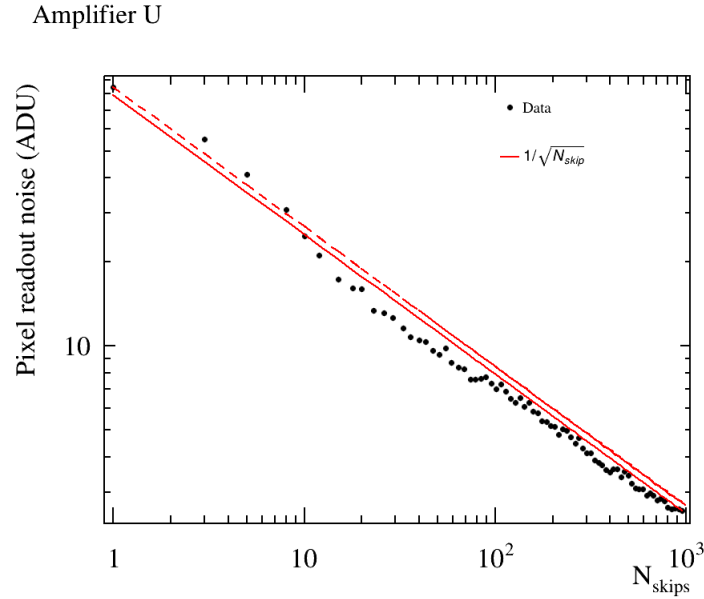


Figure 1.9: Pixel readout noise in ADUs as a function of the number of skips. The red lines correspond to the expected $1/\sqrt{N_{skips}}$ trends, the dashed one starts from the first data point whereas the last one from the last data point. Black points are measurements of the pixel readout noise for a number of skips from 1 to 1000. Image obtained thanks to the analysis software WADERS [A.2](#).

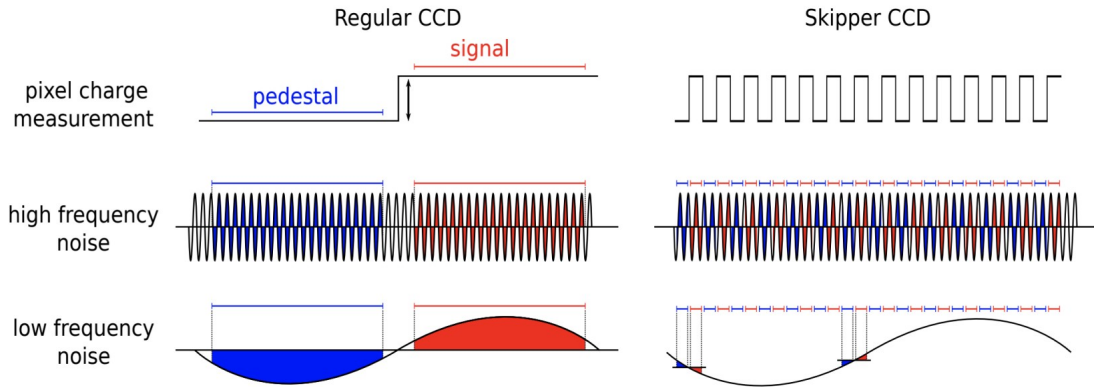


Figure 1.10: Comparison between the pixel charge measurement of a conventional versus a skipper CCD. The low-frequency noise component is visibly smaller for the skipper readout. Figure from [16].

a gate. Therefore, there is no ohmic contact that forces the charge to be flushed out when the SN is set at V_R and in consequence the SW and the OG (the output gate in conventional CCDs was a fixed bias voltage but in skipper CCDs is a clock) can change their potential values from high to low so that charge can be driven back out from the floating gate to the SW. The charge clocking process from the SW to the SN and vice versa is shown in Figure 1.11. This process can be repeated a desired number of times and in consequence pixel charge can be measured a desired number of times (“skips”).

The reset pulse only sets the SN back to V_R after charge readout. Removing the charge requires a Dump Gate (DG) and a drain voltage V_{drain} . While charge is being integrated in the Sense Node the Dump Gate is held high so that the charge does not drain, but after the last measurement this gate is lowered and charge is cleared out. In Figure 1.12 it is shown an scheme of the entire output stage structure of skipper CCDs.

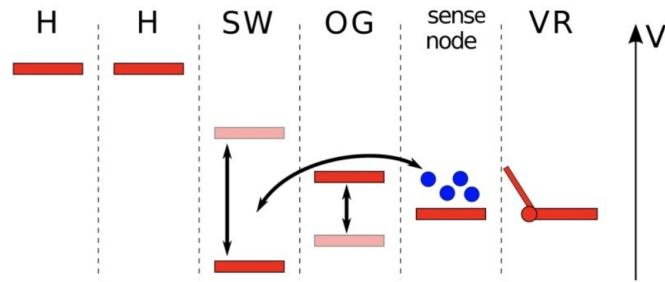


Figure 1.11: Scheme of a skipper CCD NDCM. Charge is moved from the SW to the SN trough the OG and after the readout the OG and SW voltages can be lowered so that charge can return to the SW. This entire process can be repeated for additional NDCMs. Scheme from [16].

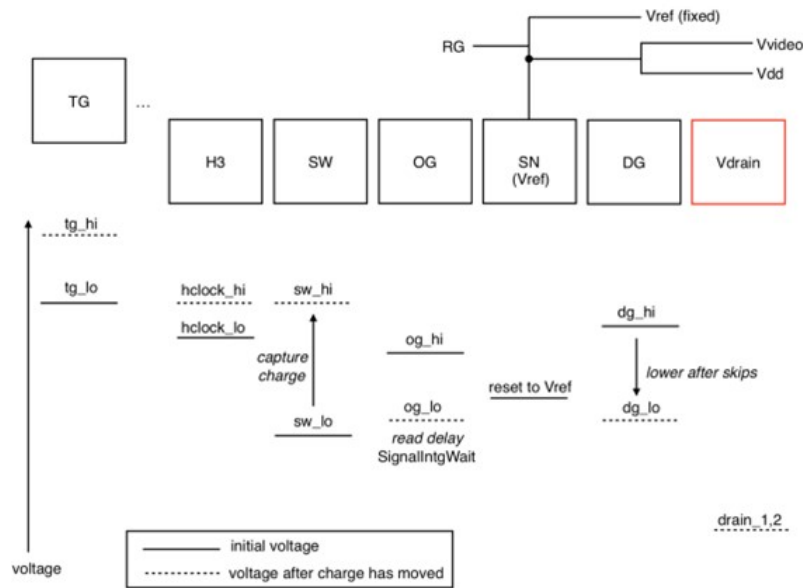


Figure 1.12: Diagram illustrating the structure of the output stage in a skipper CCD.

As it has already been mentioned, skipper CCDs achieve the sub-electron noise level due the statistical reduction of the uncertainty that results for averaging each pixel value over all the NDCMs. The information of each NDCM measurement is kept in a “raw” FITS file. To obtain the average image, the average of the NDCMs for each pixel is performed and this is done trough an analysis software such as WADERS (see A.2). In Figure 1.13 it is shown the evolution of the pixel charge distribution as the number of skips used to obtain the average image increases. Individual electron peaks are clearly seen better for a higher number of skips. The gain k can be extracted from the distance between the centroids of the first and second peaks. The 1st peak corresponds to the pixels that contain $0 e^-$, the 2nd peak refers to the pixels that contain $1 e^-$ and the 3rd peak corresponds to the pixels that contain $2 e^-$ (the term e^- is used to refer to a single unit of charge even though it is technically a hole).

To accurately quantify the dark current, it is important to identify and remove the clusters, i.e. to apply the clustering and masking processes correctly. Specifically, for the image corresponding to the dark current fit plot shown in Figure 1.14, to reconstruct the clusters (see in blue) the clustering process has performed a systematic search of the image looking for pixels with charge higher than 3σ , where σ corresponds to the readout noise. Pixels with charge above this pedestal threshold are considered as

potential clusters. If at least one pixel in each of the potential clusters contains a charge above a defined limit of 10σ , the region is definitely considered a cluster. A masking process is then performed to remove the clusters. Dark current can then be quantified by performing a Gaussian-Poisson convolution on the “de-clustered” histogram. The entire process is carried out using the WADERS analysis software [A.2](#).

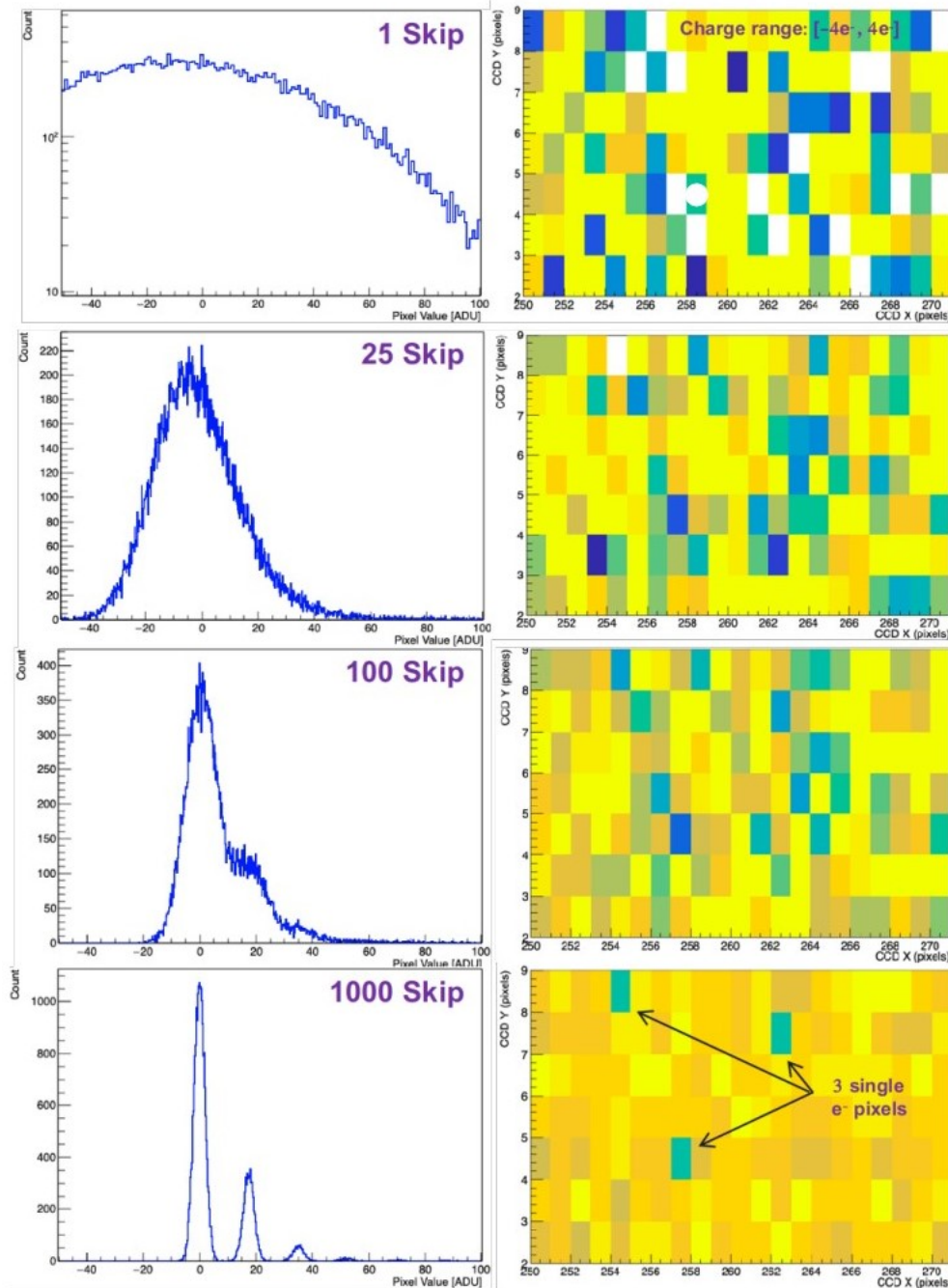


Figure 1.13: Evolution of the same Pixel Charge Distribution (PCD) and selected image region as the number of skips increases. One can see that as the number of skips increases, the PCD becomes more tighten and a discrete peak structure emerges while the noise per pixel is reduced on the image. Initially, the image region showed a wide range of potential charge values (limited to $-4e^-$ to $4e^-$ in terms of colors). After 1000 skips, the region contains only 3 occurrences of $1e^-$ events. Figure from [11].

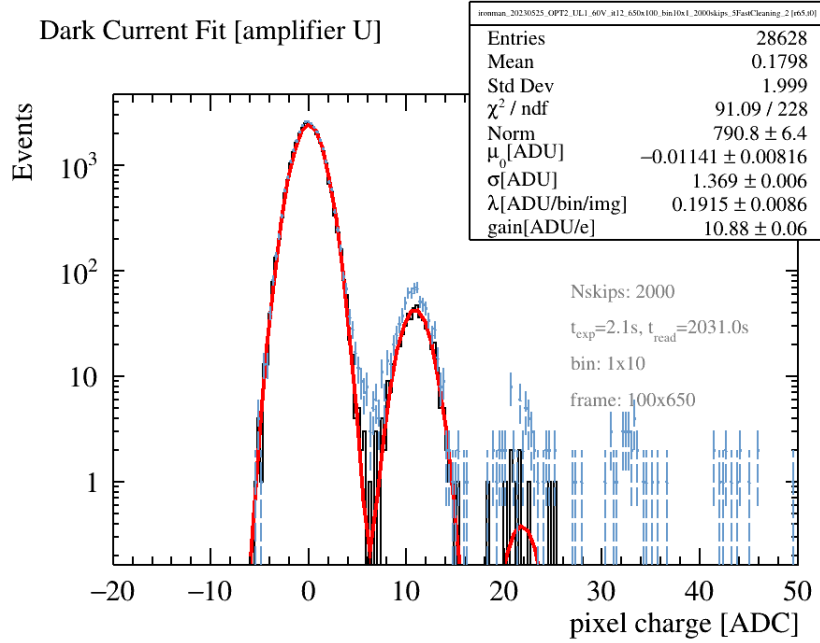


Figure 1.14: Dark current fit plot of an image taken with 2000 skips. The black histogram corresponds to the histogram after the clustering and masking processes. The dark current rate λ (given in units of ADU per binning per image), the calibration constant k and the resolution (readout noise) σ are given by the dark current fit (red curve), i.e. the Gaussian-Poisson convoluted fit of the black histogram.

1.3.2 Silicon defects in CCDs

Silicon has the basic diamond crystal structure, formed by two merged face-centered cubic lattices², where each lattice is offset from the other by $a/4$ (one-fourth of the lattice constant) in the x , y and z directions. The offset arrangement creates a three-dimensional repeating pattern. [18]

Silicon crystals can exhibit various types of defects, which are imperfections or irregularities in the crystal structure. These defects can appear during crystal growth, fabrication processes, or due to external factors. They can be classified into lattice defects, point defects, cluster defects, and precipitates. Lattice defects refer to dislocations in the crystal lattice structure. Point defects can be first classified as intrinsic or extrinsic defects. Intrinsic defects can be classified in vacancies and self-interstitial defects. Vacancies refer to positions within the crystal lattice where a silicon atom is missing and self-interstitial defects correspond to host atoms sitting in a normally unoccupied site or interstice. On the other hand, extrinsic defects (due to an impurity, i.e. foreign atoms) can be classified as substitutional (an impurity substitutes a host atom) or interstitial (an impurity occupies an empty space between host atoms). Cluster defects refer to the occurrence of groups (clusters) of defects in the silicon crystal and precipitates are clusters of impurity atoms that are segregated and form distinct regions within the silicon crystal. [18] [19]

CCDs performance can be affected by various factors, including defects in the silicon lattice. As a result of defects, traps can arise, which are localized regions within the semiconductor material where charge carriers (electrons or holes) can be captured and stored temporarily. Consequently, traps affect individual pixels and columns by producing hot or bad pixels. Hot pixels are individual pixels that show a higher dark current than the rest, while bad pixels exhibit a lower dark current. “Super-hot pixels” are

²Face-centered cubic (FCC) lattices are three-dimensional arrangements of points in which the lattice points are located at the corners of the cube and at the centers of all the faces of the cube.

pixels that saturate on the time scale of the readout process and in consequence create “hot columns”, since the neighbouring pixels that are located down the super-hot pixel in the same column pass through this pixel during the readout process. These hot columns often exhibit a characteristic behaviour called “exponential decays”. This refers to the gradual decrease in signal intensity along the length of a hot column, following an exponential function. Bad pixels can act as charge traps that absorb or trap the charge that should have been collected by the pixel. This trapped charge does not contribute to the signal readout, resulting in a reduced signal for that pixel. As a result, the affected column in the image will exhibit a dark or attenuated region corresponding to the location of the bad pixel [19].

At low temperatures, the thermal energy may not provide enough energy for significant numbers of charge carriers to occupy these traps. As the temperature increases, the thermal energy also increases, allowing more charge carriers to overcome the energy barrier and get trapped in these existing defects, which will result in the appearance of more hot or bad pixels/columns. Their increasing appearance as the temperature is raised has been studied.

1.4 Goals of this study

An experimental setup for characterizing CCDs for the DAMIC-M experiment has been established in a clean room at IFCA (Instituto de Física de Cantabria). In the DAMIC-M experiment CCDs are always operated underground. Since this setup is not located underground, CCD images have been taken by operating the CCD in such a way that the data extracted from these images simulate as closely as possible the type of data that would be extracted from images taken by a CCD experimental setup located underground. This setup, which is briefly described in Chapter 2, has been commissioned for the first time by characterizing a non-scientific skipper CCD, CCD PP52-U. Given the broad nature of CCD characterization, this study has focused on the optimization of the CCD configuration parameters and the study of the influence of the temperature in the manifestations of the traps generated by silicon defects.

Apart from the CCD characterization, the results of an additional investigation of the influence of electromagnetic noise on the quality and readout noise of CCD PP52-U is presented in Chapter 3. This analysis has revealed the high sensitivity of the CCD experimental setup to electromagnetic noise and has provided information about different electromagnetic noise sources.

The study also focuses on the optimization of the CCD configuration parameters to improve the efficiency of charge collection, transfer and readout processes. This optimization, which is presented in Chapter 4, is crucial for reducing and correctly calibrating the dark current. Consequently, more reliable estimations of the pixel readout noise are obtained.

Finally, Chapter 5 presents a study that has been conducted to explore the generation of traps caused by silicon defects, which can manifest as bad columns, hot pixels, super hot pixels and hot columns. The focus of this research is to observe their progressive appearance as the temperature increases and to analyze the changing behaviour of the hot columns with temperature.

Chapter 2

Experimental setup

The direct DM search experiments are demanding a higher sensitivity to be able to detect and distinguish potentials signals from DM interactions with ordinary matter. A Skipper CCD Test Chamber has been installed in a clean-room at the Institute of Physics of Cantabria (IFCA). This experimental setup will be dedicated to characterizing the CCD for different experiments (DAMIC-M and Oscura), specifically optimizing the CCD configuration parameters by checking the single electron resolution of the dark current measurements, studying the influence of electromagnetic noise on the CCD images, and taking images at different temperatures to gain a better understanding of the silicon defects, etc.

The experimental setup that corresponds to the Skipper CCD Test Chamber is shown in Figure 2.1. The different components required are described in the following sections.

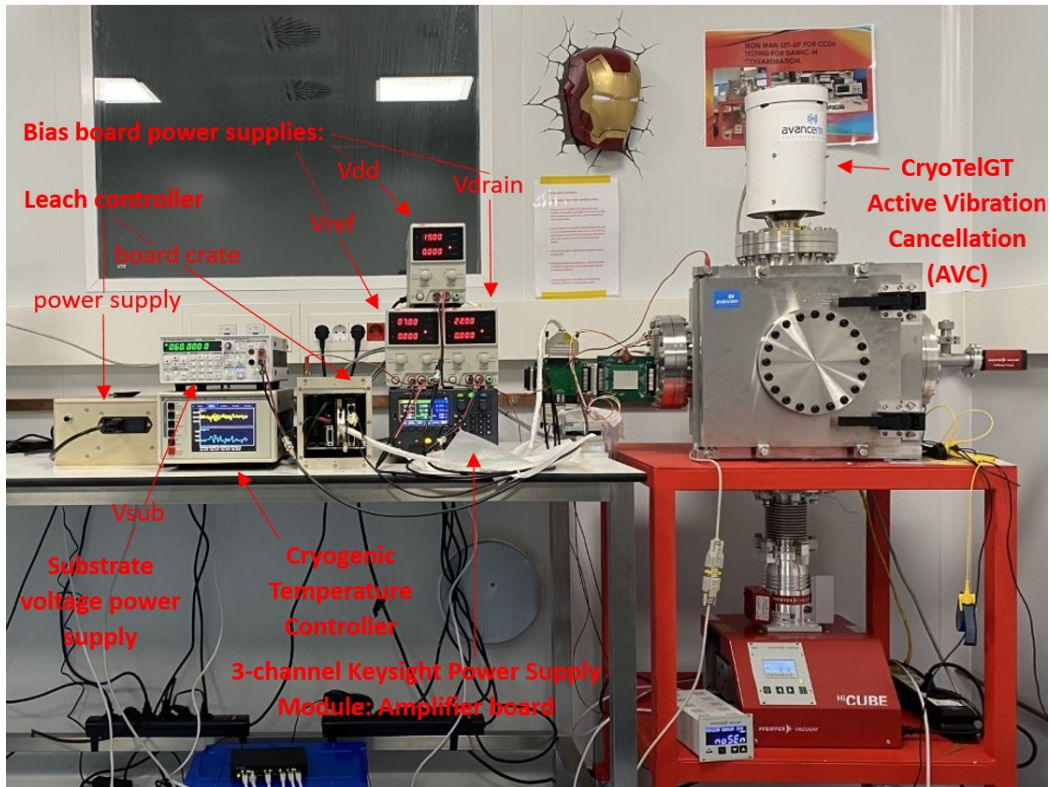


Figure 2.1: IRON MAN set-up for CCDs testing for DAMIC-M collaboration with labelled instrumentation.

2.1 Cryostat

The cryostat is an essential component of the CCD setup. Not only does it provide low temperatures to reduce noise and increase sensitivity but also ensures that the CCD is protected from the environment. The cryostat consists of a chamber, a vacuum control system, a cooling system and a temperature control

system. The chamber encloses the CCD and the kapton flex cable. The vacuum control system consists of a HiCube 80 vacuum pump that controls the air pressure inside the chamber. Pressure is monitored with a CenterOne controller, which measures the pressure inside the chamber with a pressure gauge. The CCD box is supported inside the chamber by an L-shaped copper structure which is affixed to the cold head of the cryocooler using screws. The cooling system mechanism, which is a cryocooler, is used to lower the temperature of the CCD through the copper support. To mitigate potential mechanical stress and electronic noise induced by vibrations at the cold head, the cryocooler is equipped with an active vibration cancellation (AVC) system. This system effectively minimizes vibrations and ensures stable operation of the CCD. The cryocooler (CryoTelGT) can not regulate the temperature, so a temperature control system, i.e. the Cryogenic Temperature controller (CTC100), is needed for that. This system includes a temperature sensor and a power heater that ensures that the desired temperature is achieved. Specifically, the temperature is set at 120 K. The purpose of cooling a CCD is to reduce dark current, which can interfere with the signal-to-noise ratio of the CCD. [4]

2.2 Electronics

The skipper CCD system features several standardized air-side electronics. The CCD controller (LEACH) within the system incorporates PCBs to deliver clock signals to the CCD based on a user-defined sequencer (the CCD sequencer provides the timing waveforms defining exposure, transfer and readout phases). A grounding wire is connected from the LEACH to the chamber/camera of the CCD. This connection serves to establish an electrical ground reference between the two components. The grounding wire helps to ensure proper electrical grounding since it provides a reliable and low-resistance path for electrical currents. Due to delays in the arrival of electronic components for the bias board, it was not possible to complete its construction on time. Therefore, a “house made” bias board is implemented for the LEACH system, which consists on three power supplies to provide voltages for V_R (reference voltage), V_{dd} (amplifier voltage) and V_{drain} (drain voltage). Furthermore, the LEACH is responsible for processing and digitizing outputs from CCD video channels. The second-stage PCB is responsible for shaping the clock signals from the controller and amplifying the CCD video signal. A breakout PCB is used to rout clock, bias and video signals in and out the second stage board (Figure 2.2 provides a close-up view of both boards). Power supplies are allocated for the second-stage amplification (3-channel KeysightE36312A Power Supply in Figure 2.1) and CCD substrate voltage (Substrate voltage power supply in Figure 2.1). Communication between computer and controller is achieved using fiber optic cables.

2.3 Detector

The cryostat described previously has been used to operate a 6k x 1.5k non-scientific skipper CCD (see Figure 2.3) with four read-out amplifiers (located at both ends of the two outermost rows, i.e. the serial registers), which can be used individually or collectively to acquire images. However, due to the limitation of having only one available readout system, only two amplifiers can be used simultaneously to read the CCD. The CCD is equipped with a short flex wirebonded and has a 50-pin D-Sub female connector on one end. To establish a connection between the CCD and the feedthrough vacuum side, a Kapton flex cable with 50-pin male (CCD) and female (feedthrough) connectors is utilized (not shown in Figure 2.3). Once all necessary adjustments are made, the chamber door-plate is secured, and the vacuum is created. The temperature is set to 120 K, and once the system reaches cryogenic stability, the detector operation can commence.

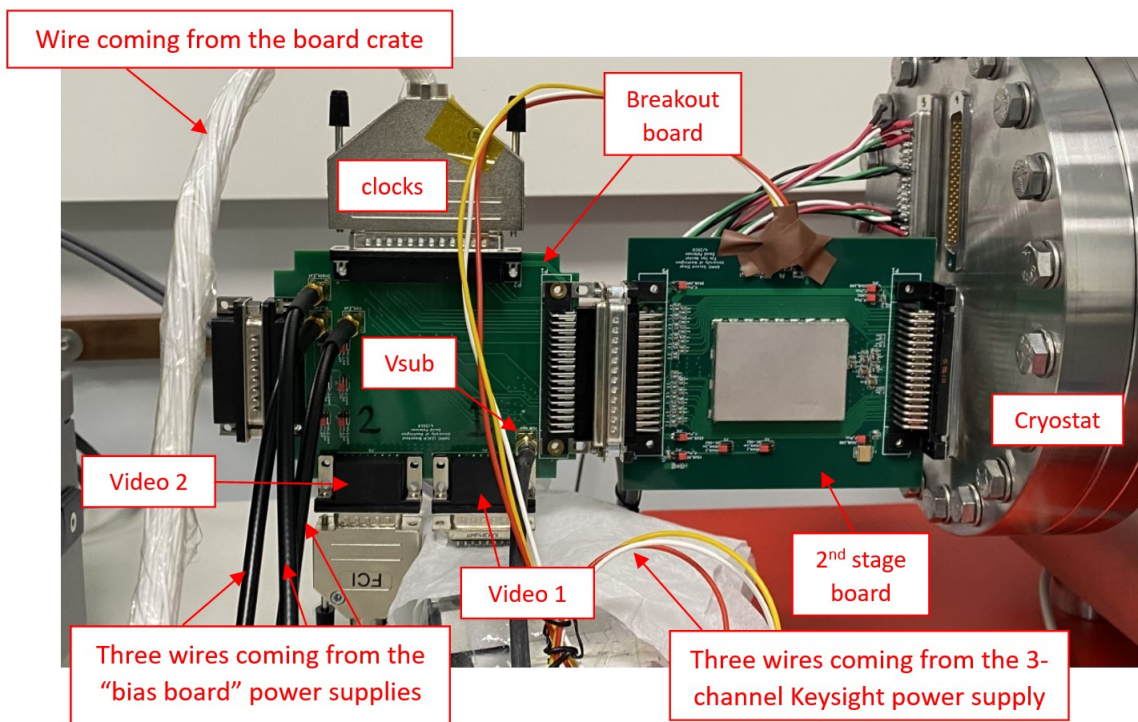


Figure 2.2: Breakout and second-stage boards are shown with labelled features.

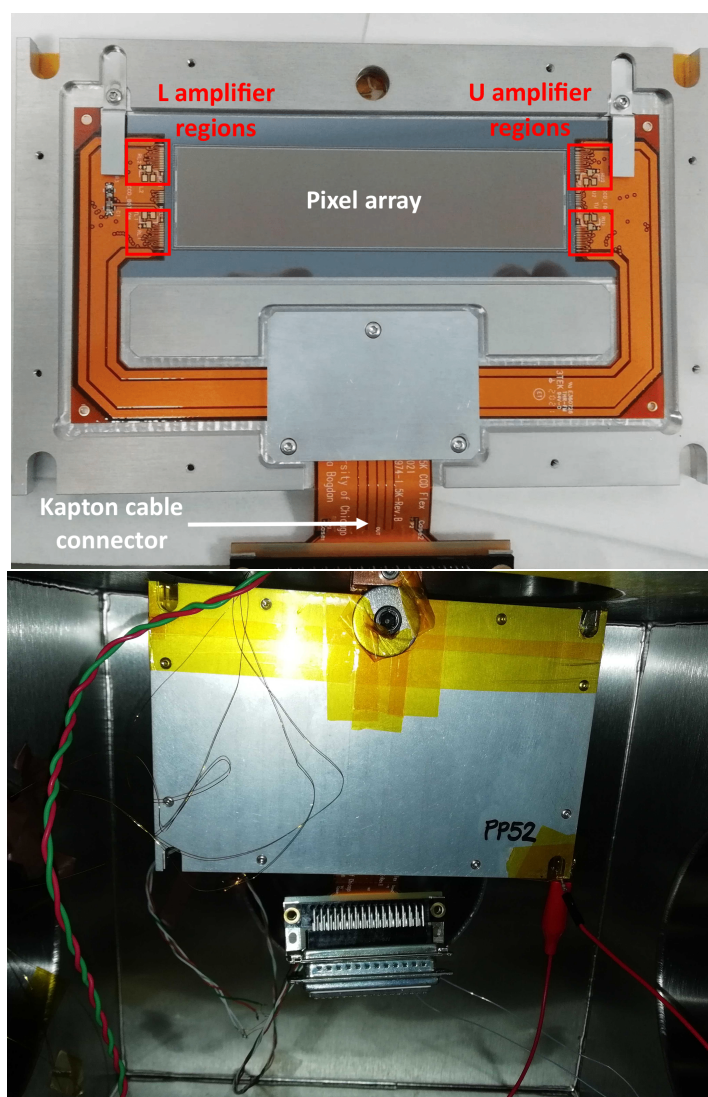


Figure 2.3: CCD PP52-U images in its aluminum box. In the above image some features have been labelled. In the below image the CCD is screwed to the copper support inside the cryostat test chamber.

2.4 Remote control of operational parameters

Slow control (SC) and data acquisition (DAQ) machines are two separate components used in this experimental setup for control and data collection purposes.

2.4.1 Slow Control System

The Slow Control system enables remote operation and monitoring of key parameters and instruments involved in the CCD setup through the [SC web interface](#)¹. The user can switch on/off the instruments and adjust the values of different parameters. These are the power output controlled by AVC, the Amplifier +/- board voltages and the ramp rate and setpoint temperature of the CTC 100 heater. Moreover, this web provides real-time information about the system's status. The user can monitor the values of the mentioned parameters and visually track their time evolution through graphical representations. Furthermore, several instruments can be reset, such as the Center One controller, CTC 100, CryoTelGT and KeysightE36312A. It is important to note that the SC system does not currently control and run the vacuum pump (HiCube80) as it has not been integrated into the SC system.

2.4.2 Data Acquisition (DAQ) machine

The DAQ machine is responsible for acquiring, processing, and storing data from the CCD. The DAQ machine receives the analog output signals from the CCD and performs an analog-to-digital conversion to convert them into digital data that can be processed and analyzed by a computer. The acquired CCD data is stored in an image FITS file. The DAQ machine transfers the data to a computer for further analysis or storage. With the computer, the CCD configuration parameters² can be specified and the data acquisition process can be controlled. In the appendix section [C](#) a guide to skipper CCD Start Up and data-taking with the LEACH DAQ system CCDDrone can be found.

¹http://gaepc6.ifca.unican.es/SC_web/slow_control_set_vals.php

²CCD configuration parameters are shown in the appendix section [B](#).

Chapter 3

Study of non-electronic noise sources for the CCD PP52-U experimental setup

The main objective consisted on the optimization of CCD PP52-U configuration parameters to achieve an efficient charge collection, transfer and readout; which consequently leads to an improvement of the electronic noise. In order to determine the optimal configuration parameters, the integration time was initially varied, which resulted in finding that the CCD Test Chamber installed at IFCA presents a high sensitivity to electromagnetic noise. This discovery prompted an investigation into how this electromagnetic noise visually impacts the images, the pixel readout noise and the dark current fit plots. Therefore, in the following subsections, which correspond to the non-skip and skip images cases, it is presented how the initial variation of the integration time parameter led to the discovery of several electromagnetic noise sources.

Due to lack of time to optimize the parameters of the L amplifier, the analysis has been carried out only with the results obtained from the U amplifier, since the different configurations of parameters used provide better results for the images taken with this last one. The CCD experimental setup at IFCA is not located underground. Consequently, the CCD receives numerous particle impacts. To try to simulate as closely as possible the data acquisition process of an underground setup only the CCD serial register has been read for all the images taken. By reading only the serial register, the amount of charge read is significantly minimized, as any charge that has accumulated in the active region during the exposure time is not read. Reading this region would result in a significant increase in the number of particles being read, which is not representative of the conditions encountered by CCDs in underground setups. Therefore, charge from the active region has been clocked towards the opposite serial register, i.e. the one with the unused amplifiers. Thus, besides the dark current, the only charge that should be read is due to particles arriving at the serial register during the readout and exposure time.

3.1 Non-skip images

The integration time parameter has been initially varied in order to find the value at which the pixel readout noise σ is the lowest. To conduct the study of this parameter, the pixel readout noise as a function of the integration time distribution obtained during the initial commissioning of the IFCA setup was used as a reference. This distribution, acquired on 21/09/2022, will be referred to by its date for the remainder of the study. The same study was then conducted on 08/02/2023, i.e. new non-skip images were taken with the same configuration parameters and varying the integration time. It is important to note that by late September 2022, there was poor thermal insulation, meaning that the CCD was at a higher temperature and was not electrically isolated from the vacuum pump. However, by February, these issues had been resolved, which resulted in a plot of the noise versus the integration time with significantly lower noise for the different integration times compared to the reference plot. Both curves depicting the pixel readout noise in units of e^- as a function of the integration time are presented in

Figure 3.1. The analysis software WADERS A.2 provides the pixel readout noise σ in ADUs (Analog-to-Digital units) by fitting a Gaussian distribution to the overscan pixels. In order to obtain this magnitude in units of electrons (e^-) a conversion is necessary. The conversion is the gain k (ADU per e^-), explained in Chapter 1. To determine the value for non-skip images, an external radiation source like ^{55}Fe can be utilized¹, but unfortunately, it is not available. However, for skip images, obtaining the value of k is a straightforward process. It involves fitting the dark current of a pixel's charge distribution and measuring the distance between the 0 and 1 e^- peaks. Therefore, the value of k for each value of the integration time for non-skip images has been estimated by obtaining the average of five measurements of k obtained from five skip-images. It is necessary to average at least five measurements because k exhibits some fluctuations in skip-images. The error of k is determined as the standard deviation of the five measurements.

Curves shown in Figure 3.1 exhibit significant differences, not only in terms of noise levels but also in terms of shape. Until a value of approximately 12 μs the curve corresponding to the old case (images from 21/09/2022) decreases while the one corresponding to the new case (images from 08/02/2023) shows the opposite behaviour. For values approximately higher than 12 μs both curves begin to increase.

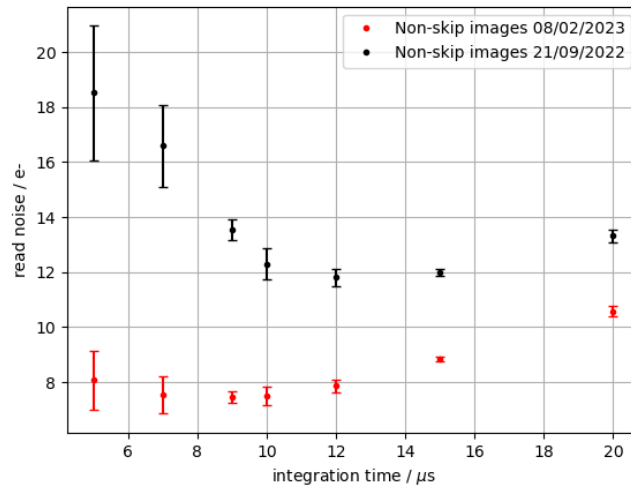


Figure 3.1: Single-skip pixel readout noise σ in units of e^- as a function of the integration time for non-skip images taken on 21/09/2023 (black dots) and on 08/02/2023 (red dots). The error bars of the data points have been determined by propagation of errors taking into account the error of σ in ADUs (error of the standard deviation of the Gaussian distribution fitted to the overscan pixels) as well as the error estimated for the gain k (standard deviation of 5 measurements of k from skip-images).

Figure 3.2, from Miguel Sofo Haro's thesis [13], illustrates a similar difference in curvature and noise for two cases where the only distinction was the presence or absence of correlated noise in the images. Correlated noise in CCD images can arise from electromagnetic noise sources that introduces noise into the system. This noise can manifest in the images as a series of noise patterns that exhibit a relationship or correlation between neighboring pixels or regions within the image.

Therefore, the lack of proper thermal and electrical insulation of the CCD in September 2022 could be a cause of the appearance of correlated noise. Consequently, this could explain the observed fluctuation in curvature between the curves from Figure 3.1. To confirm this, on 16/02/2023, images were taken with the grounding cable disconnected in order to generate correlated noise. The grounding wire helps

¹See [20] for more information.

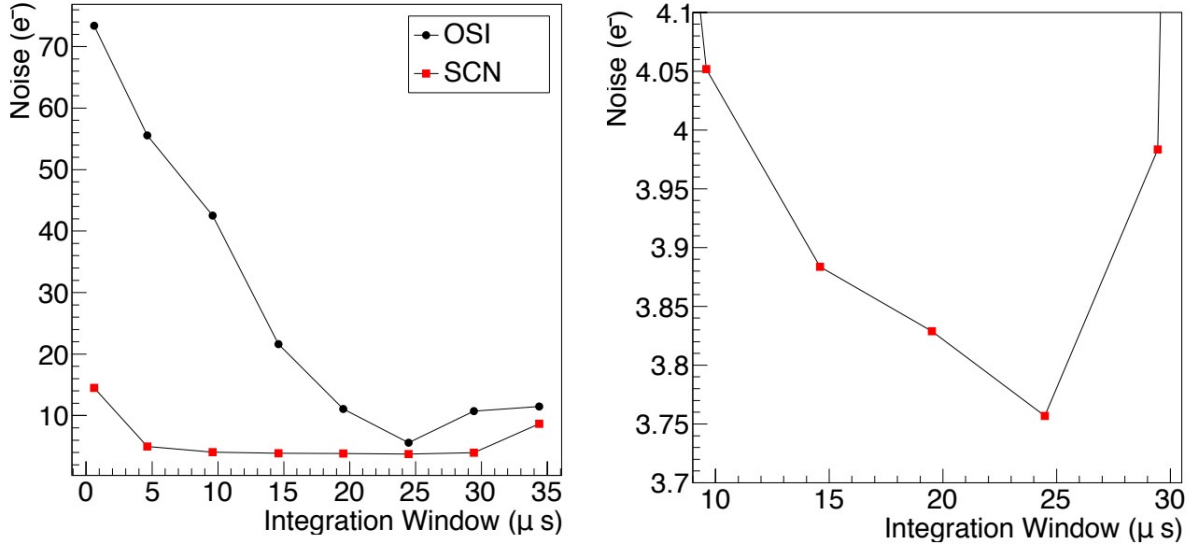


Figure 3.2: Single-skip noise as a function of the integration time. The measurement of the readout noise was performed by fitting a Gaussian distribution to the overscan pixels. In the left plot, the curve with black dots represents the noise of the images after subtracting the overscan, while the curve with red dots represents the noise after subtracting both the overscan and the correlated noise. The right plot corresponds to a zoomed-in view of the left plot. Figure from [13].

divert any unwanted electrical interference or noise that may be present in the system. This element can help to reduce the impact of electromagnetic interference or other sources of correlated noise that could affect the CCD sensor or the image acquisition process. The curve from Figure 3.3 exhibits a highly similar behavior to the one from the reference plot (plot from 21/09/2022).

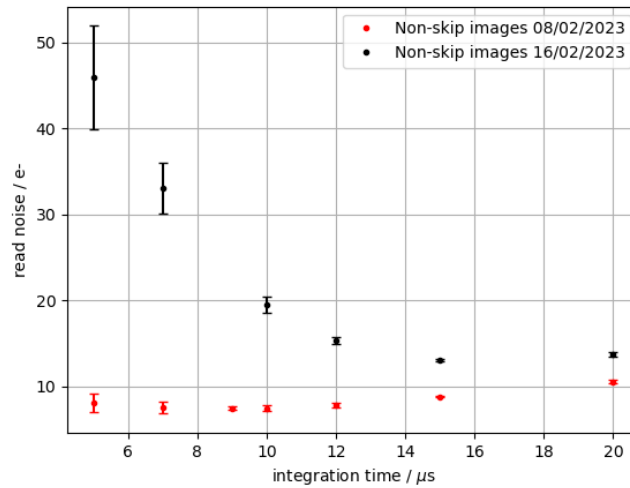


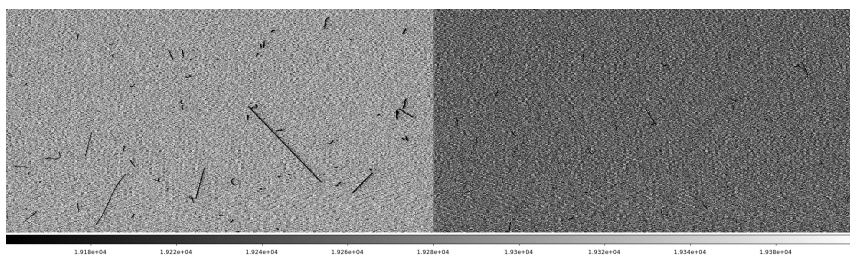
Figure 3.3: Single-skip readout noise as a function of the integration time for non-skip images taken on 16/02/2023 (black dots) and on 08/02/2023 (red dots). The error bars of the data points have been determined by propagation of errors taking into account the error of σ in ADUs (error of the standard deviation of the Gaussian distribution fitted to the overscan pixels) as well as the error estimated for the gain k (standard deviation of 5 measurements of k from skip-images).

Finally, a comparison has been done between the images that correspond to the three cases explained. Images from 21/09/2022 correspond to the old setup, where inadequate thermal and electrical isolation led to the appearance of correlated noise on the images. Images from 08/02/2023 and 16/02/2023 refer

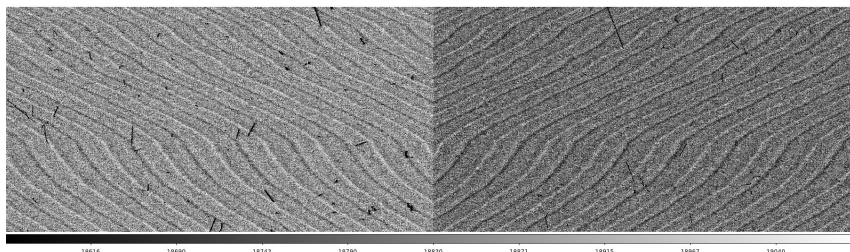
to the cases in which the thermal and electrical isolation had been improved but the difference between these two relies that the images from 16/02/2023 were taken intentionally with high correlated noise (grounding wire disconnected) while the ones from 08/02/2023 were not. Images from 08/02/2023 were expected to be free from correlated noise patterns due to the improved thermal and electrical isolation in the experimental setup, including the connection of the grounding wire.

Figure 3.4 shows two images for each of the three cases (21/09/2022, 16/02/2023 and 08/02/2023) at two different values of the integration time. There is a noticeable difference between the images taken on 21/09/2022 and 16/02/2023 compared to those taken on 08/02/2023. The presence of noise patterns in the first two cases results in a significant increase in noise compared to the third case, as reflected in Figures 3.1 and 3.3. In these figures the black dots represent images with high correlated noise whereas the red dots correspond to images with negligible correlated noise. Therefore, the observations depicted in Figure 3.2 are corroborated.

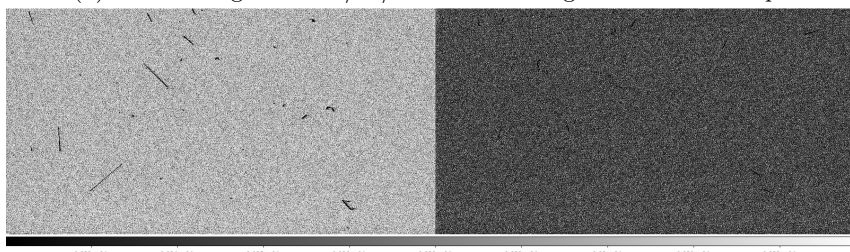
However, as illustrated in Figure 3.4, some of the images from 08/03/2023 show correlated noise patterns. This Figure shows a particular case where low correlated noise is observed for an integration time of 15 μs but not for 5 μs . Therefore, there is an additional source of noise that introduces a lower level of correlated noise on the images compared to the other mentioned noise sources. This unidentified electromagnetic noise source operates intermittently, as the correlated patterns are not consistently present in all the images from 08/02/2023, unlike the images taken on 21/09/2022 and 16/02/2023. The presence of this unknown electromagnetic noise source has also a minimal impact on the noise compared to a non-skip image taken when the external noise source is not working.



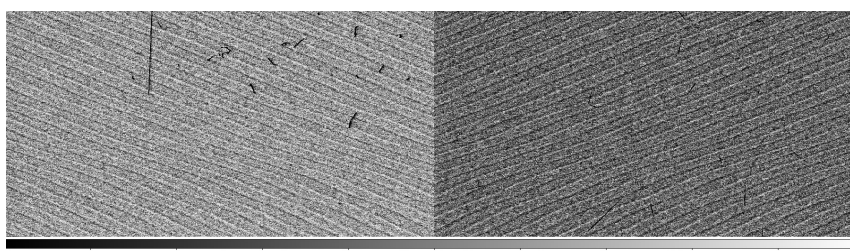
(a) “DS9” image from 21/09/2022 for an integration time of 5 μ s.



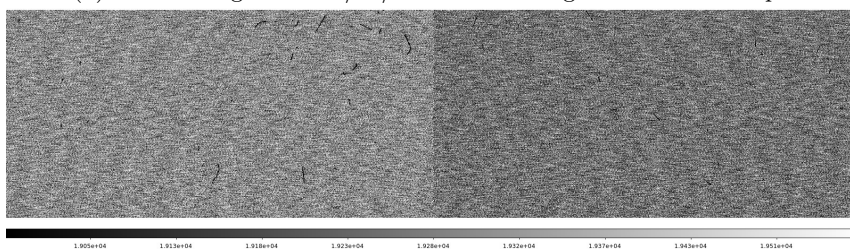
(b) “DS9” image from 21/09/2022 for an integration time of 15 μ s.



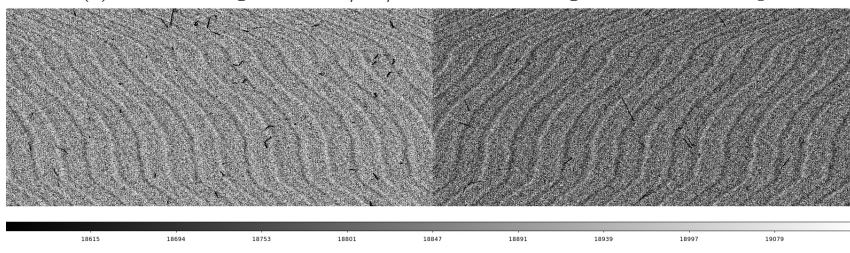
(c) “DS9” image from 08/02/2023 for an integration time of 5 μ s.



(d) “DS9” image from 08/02/2023 for an integration time of 15 μ s.



(e) “DS9” image from 16/02/2023 for an integration time of 5 μ s.



(f) “DS9” image from 16/02/2023 for an integration time of 15 μ s.

Figure 3.4: Images visualized with the “DS9 tool (explained in A.1) for two different values of the integration time, taken on three different days: September 21, 2022; February 8, 2023; and February 16, 2023.

3.2 Skip images

A study was initiated to optimize the integration time parameter for skipper CCD images. Therefore, the pixel readout noise as a function of the integration time plot has been obtained for the skipper images case. Nevertheless, when varying the integration time a series of unexpected tracks appeared in some of the images. In all these images only the serial register was being read since charge from the active region was being clocked towards the unused amplifiers. Consequently, only horizontal tracks were expected to be seen, as some particles could have reached the serial register during the exposure and readout time. These unexpected tracks have been labeled as “ghost tracks”.

Skip images, due to the multiple measurements of the same pixel charge (skips), take a longer time to be readout than non-skip images, and in consequence FITS files are also higher in size. Therefore, to ensure sufficient data storage and reduce readout time, skipper images are taken with a smaller number of rows in comparison to the size of the CCD. Due to this reduction in image size, charge can be accumulated in the pixels that are not read, leading to residual charge in the subsequent image. To avoid this issue, the acquisition strategy employed for taking skipper images involves cleaning the CCD of residual charge accumulated from previous acquisitions before acquiring a new skipper image.

The cleaning procedure involves taking an image reading the full size of the CCD without skips while sending the charge in the vertical direction to the opposite amplifiers, i.e. the ones that are not being used to read the CCD. This specific image is commonly referred to as “cleaning image” and a few of these are taken before acquiring the next skip image to ensure that any remaining charge is flushed away. To expedite the cleaning procedure, “cleaning images” are taken with an aggressive pixel binning (20 x 20).

The presence of these “ghost tracks” in the images is random, and, when present, the image noise increases. That is, under the same configuration parameters, sometimes these tracks were observed and sometimes not. At first, it was noted that they appeared when an experimental setup located in an adjacent clean room to the one that includes the CCD experimental setup, was in operation. This setup includes power sources and a laser. Therefore, it was concluded that the appearance of the “ghost tracks” was due to electromagnetic noise that was being introduced into the CCD experimental setup because of the operation of the mentioned adjacent experimental setup. The electromagnetic noise leads to correlated noise, which manifests as noise patterns when a low number of skips is used. The occurrence of these patterns increases proportionally with the number of skips until a threshold is reached, at which point the correlated noise manifests as the mentioned “ghost tracks”, as depicted in Figure 3.5. This manifestation is simply the outcome of averaging with a high number of skips in images with significant correlated noise. The increase in correlated noise in the images as the number of skips increases is attributed to the consequent increase in the readout measurement time and the improvement of the resolution of the image, i.e. the CCD experimental setup is more sensitive to external noises.

In order to avoid the presence of correlated noise in the images, it was decided to take images at nighttime, since during this period of time the other experimental setup was not operational. Unexpectedly, initial observations revealed that nighttime images had an increase in noise with respect to those taken during the daytime when the other experimental setup was not operational. A potential explanation of this event could be the fact that the adjacent clean room is turned off at 10:00 pm everyday. To confirm this hypothesis, the decision was made to keep the adjacent cleanroom operational for two consecutive

nights and take images during those periods. Surprisingly, the subsequent analysis demonstrated that some images showed no discernible difference in noise between evening and night, while others did. This observation indicated that the additional noise seen in the images in the initial observations was not due to the shutdown of the adjacent cleanroom.

Further tests were conducted by taking images both during nighttime and daytime (making sure the images were not taken when the adjacent experimental setup was operational). These tests confirmed that, in certain cases, the noise in the images was actually observed during the day rather than at night, and vice versa. As a result, it was concluded that the additional noise present in some images comes from an external noise source that does not operate continuously, which explains the absence of this noise in certain images. This unknown external noise source introduces electromagnetic noise into the CCD experimental setup, i.e. at a large number of skips “ghost tracks” were also observed in the images. Figure 3.6 shows dark current fit plots² that correspond to images taken during nighttime and daytime. It is evident that the noise σ in cases (a) and (e) is lower compared to the others, and this can be attributed to the external noise source not being operational in these cases. Case (a) corresponds to a daytime image, whereas case (b) corresponds to a nighttime image, thus confirming that the operation of this noise source is independent of the time of day.

Therefore, not only do the “ghost tracks” appear when the adjacent experimental setup is operational but also when the unknown external noise source is working. Figure 3.7 presents a comparison of three cases that correspond to three images taken with the same configuration parameters. The first one corresponds to the case in which the adjacent experimental setup was operational, in the second case the external noise source was active and in the third case neither of them were working. A clear distinction can be observed between the first two cases and the third case in terms of the presence of the aforementioned “ghost tracks” in the DS9 images and the noise σ given by the dark current fit plots. In the third case, the single electron resolution of the peaks from the pixel charge distribution improves and consequently the noise is lower.

²The legend of each of the subfigures of Figure 3.6 is too small. The same occurs with several plots presented in this document. If significant parameters are needed to understand the explanations, they will be provided in the captions. In this specific case, σ is provided in all of the subfigure captions.

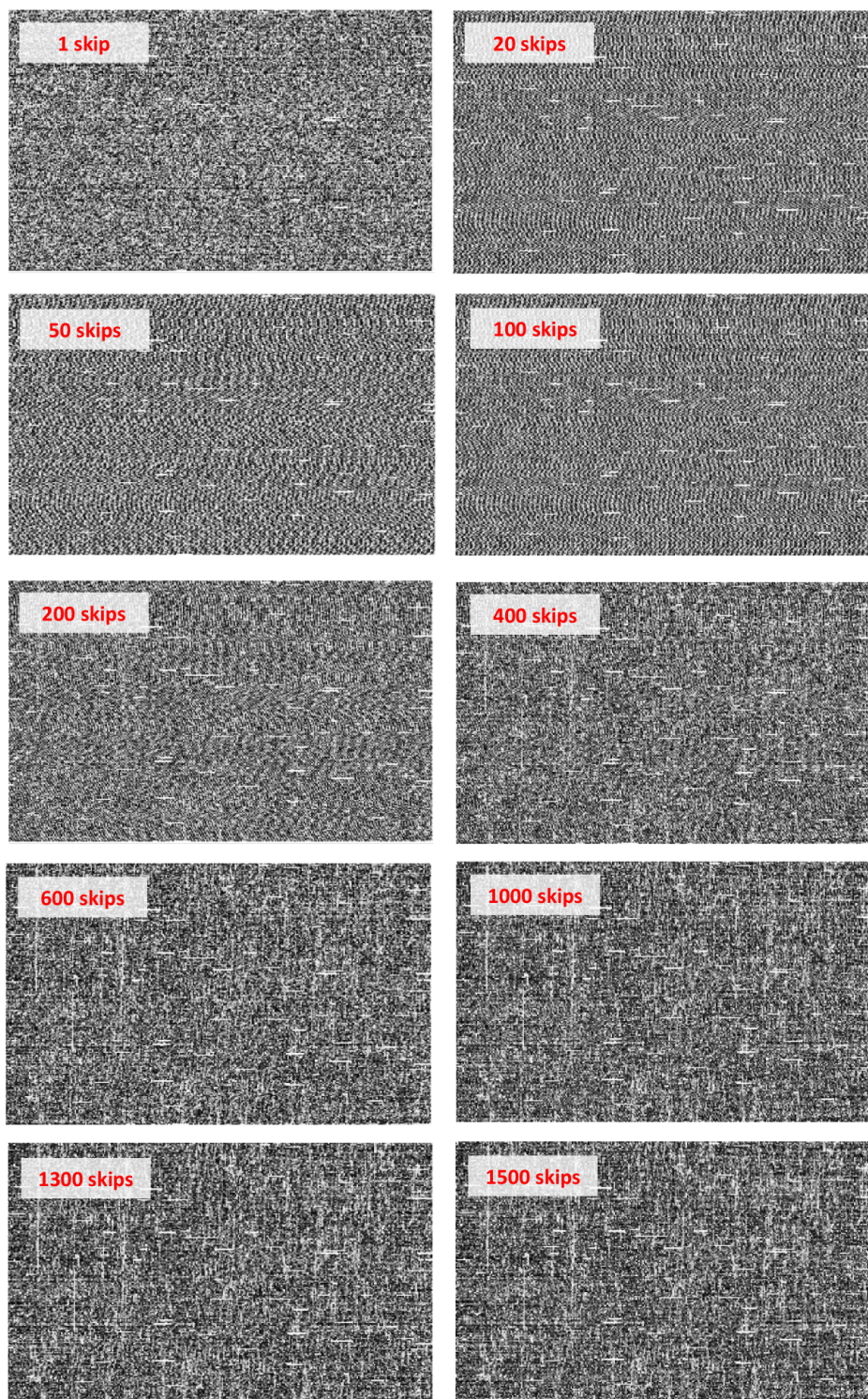
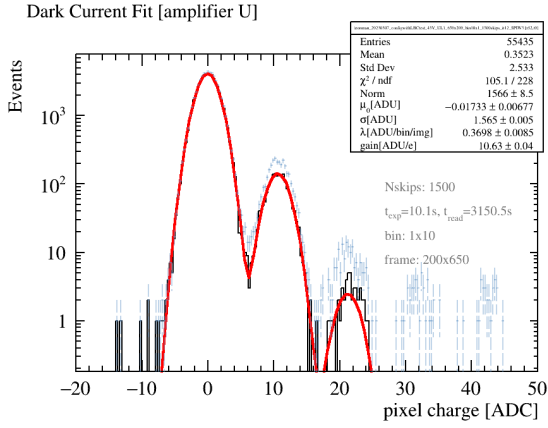
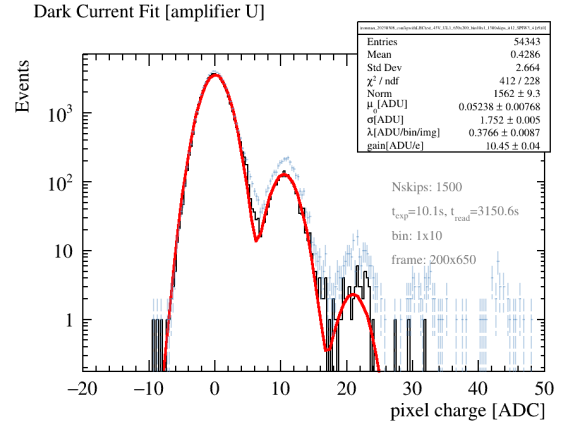


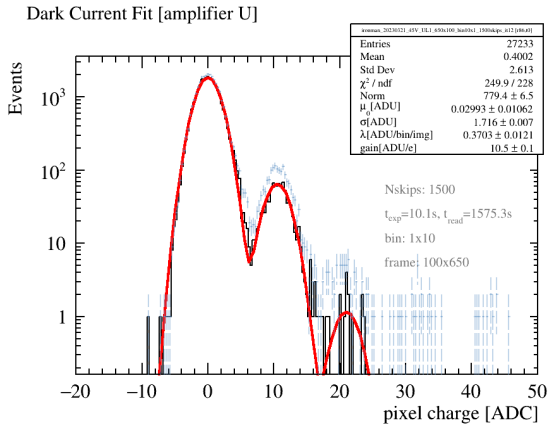
Figure 3.5: Evolution with the number of skips of an image taken originally at 1500 skips when the experimental setup of the adjacent clean room was operational. The visualization tool used is “DS9” (see A.1). The analysis software WADERS (see A.2) has allowed to reprocess the image taken originally with 1500 skips at different lower values of skips as well as subtracting the pedestal in all of them.



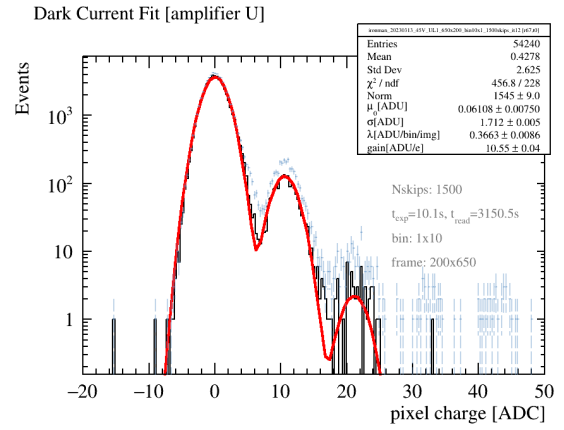
(a) Dark current fit plot of an image taken on 07/03/2023 during daytime. The noise is $\sigma = (1.573 \pm 0.005)$ ADU.



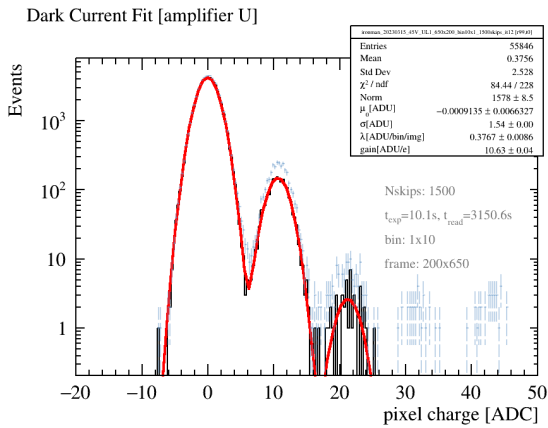
(b) Dark current fit plot of an image taken on 08/03/2023 during daytime. The noise is $\sigma = (1.779 \pm 0.005)$ ADU.



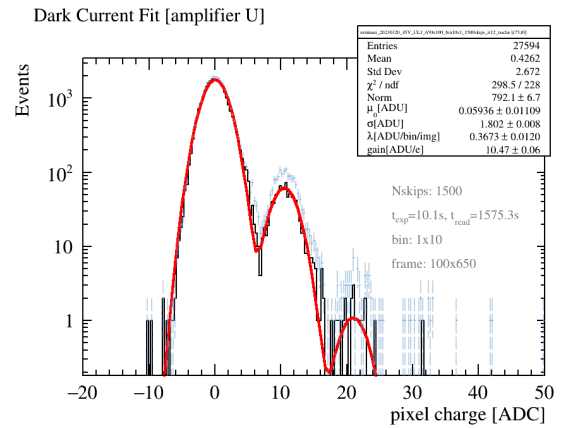
(c) Dark current fit plot of an image taken on 21/03/2023 during daytime. The noise is $\sigma = (1.752 \pm 0.005)$ ADU.



(d) Dark current fit plot of an image taken on 13/03/2023 at night. The noise is $\sigma = (1.785 \pm 0.005)$ ADU.

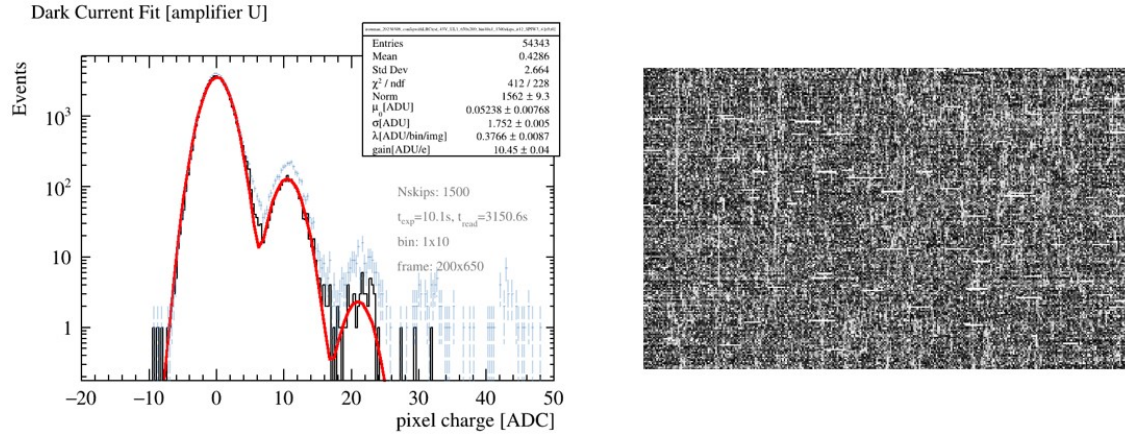


(e) Dark current fit plot of an image taken on 15/03/2023 at night. The noise is $\sigma = (1.571 \pm 0.005)$ ADU.

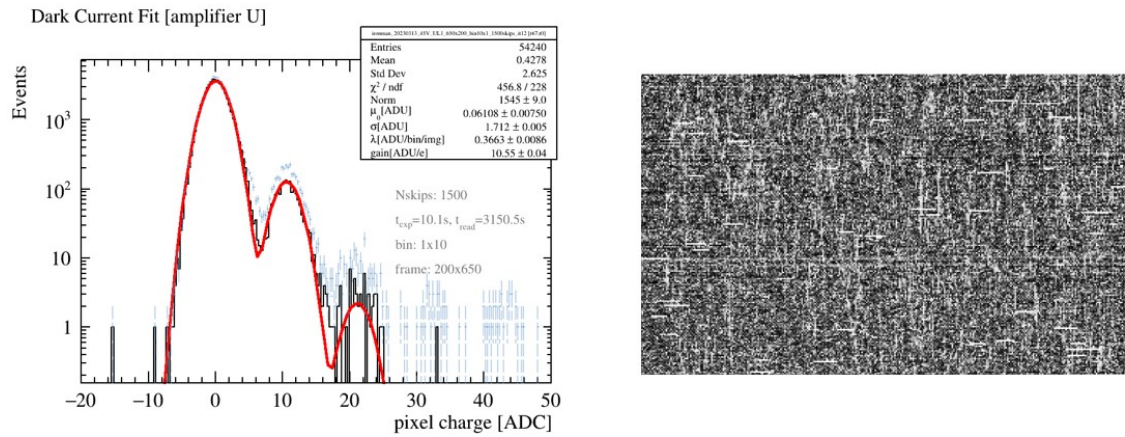


(f) Dark current fit plot of an image taken on 20/03/2023 at night. The noise is $\sigma = (1.841 \pm 0.005)$ ADU.

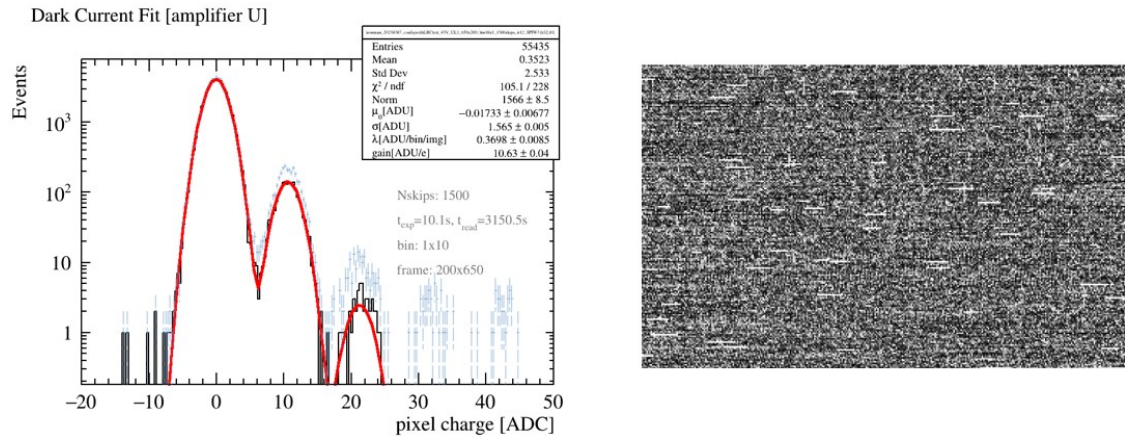
Figure 3.6: Dark current fit plots that correspond to images taken with the same configuration parameters and when the experimental setup from the adjacent clean room was not operational. The exposure time of the CCD is 10 s.



(a) Dark current fit plot and “DS9” visualization of the 1500 skips pedestal subtracted image shown in Fig. 3.5. These plots corresponds to an image taken when the experimental setup from the adjacent cleanroom was operational. The noise is $\sigma = (1.779 \pm 0.005)$ ADU. The exposure time is set at 10 s.



(b) Dark current fit plot and “DS9” visualization of a pedestal subtracted image taken when the unknown external noise source was operational. The noise is $\sigma = (1.785 \pm 0.005)$ ADU.



(c) Dark current fit plot and “DS9” visualization of a pedestal subtracted image taken when neither the adjacent experimental setup nor the unknown external noise source were operational. The noise is $\sigma = (1.573 \pm 0.005)$ ADU.

Figure 3.7: Dark current fit plots and “DS9” visualizations of images that have been taken with the same configuration parameters. The exposure time of the CCD is 10 s.

Finally, regarding the plot depicting the relationship between the pixel readout noise and the integration time, integration time plot, the influence of intermittent operation of an unidentified external noise source has been observed. This phenomenon results in varying curves each time the plot is reproduced

and even to a deviation of the points from the expected trend within each curve. Figure 3.8 shows the results of measurements taken on different days. It is evident that the noise levels do vary, especially for low integration times, but the overall trend of the curves remains relatively consistent.

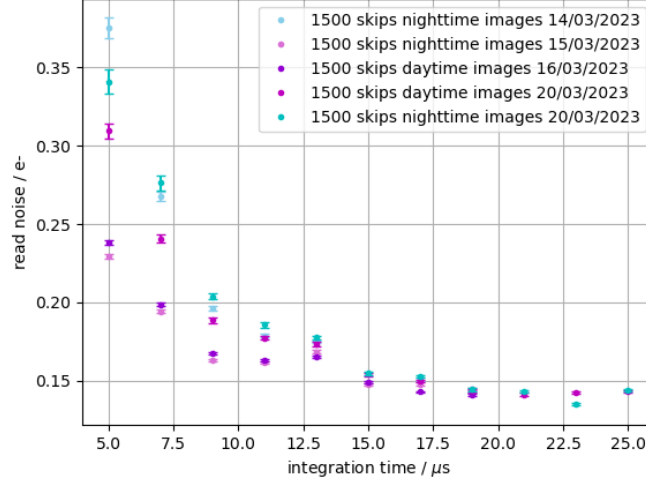


Figure 3.8: Read noise as a function of the integration time for 1500 skips images taken on different days. The dots represented on this figure correspond to the noise of images taken when the adjacent experimental setup was not operational. The error bars of the data points have been determined by propagation of errors taking into account the error of σ in ADUs as well as the of the gain k , which are obtained from the dark current fit plots

There is another electromagnetic noise source that has been found to affect CCD images. It has been observed that the CCD is highly sensitive to the arrangement of multiple wires responsible for controlling the electronic instruments within the CCD experimental setup. In particular, when the wires come into contact with each other, electromagnetic noise is introduced into the system, and this results in obtaining plots such as the ones shown in Figure 3.9. Therefore, this figure illustrates the consequences of an inadequate wire isolation. Due to the small size of the images (650 x 20), the “DS9” images are not shown. Instead, the figure presents plots illustrating the relationship between pixel readout noise and the number of skips. A non-linear trend and saturation of the noise can be seen after a certain number of skips. The saturation phenomenon occurs because as the number of skips increases, the CCD’s resolution also improves. Consequently, the CCD experimental setup becomes more sensitive to electromagnetic noise, which results in reaching a point at which increasing the number of skips no longer results in reducing the noise. Regarding the dark current fit plots, it is evident that the dark current fitting is inaccurate, as the distribution peaks do not follow a Gaussian-Poisson convoluted distribution. To effectively prevent this generation of electromagnetic noise that adversely affect CCD images, it is crucial to either separate the wires or use kapton tape to ensure proper isolation between them.

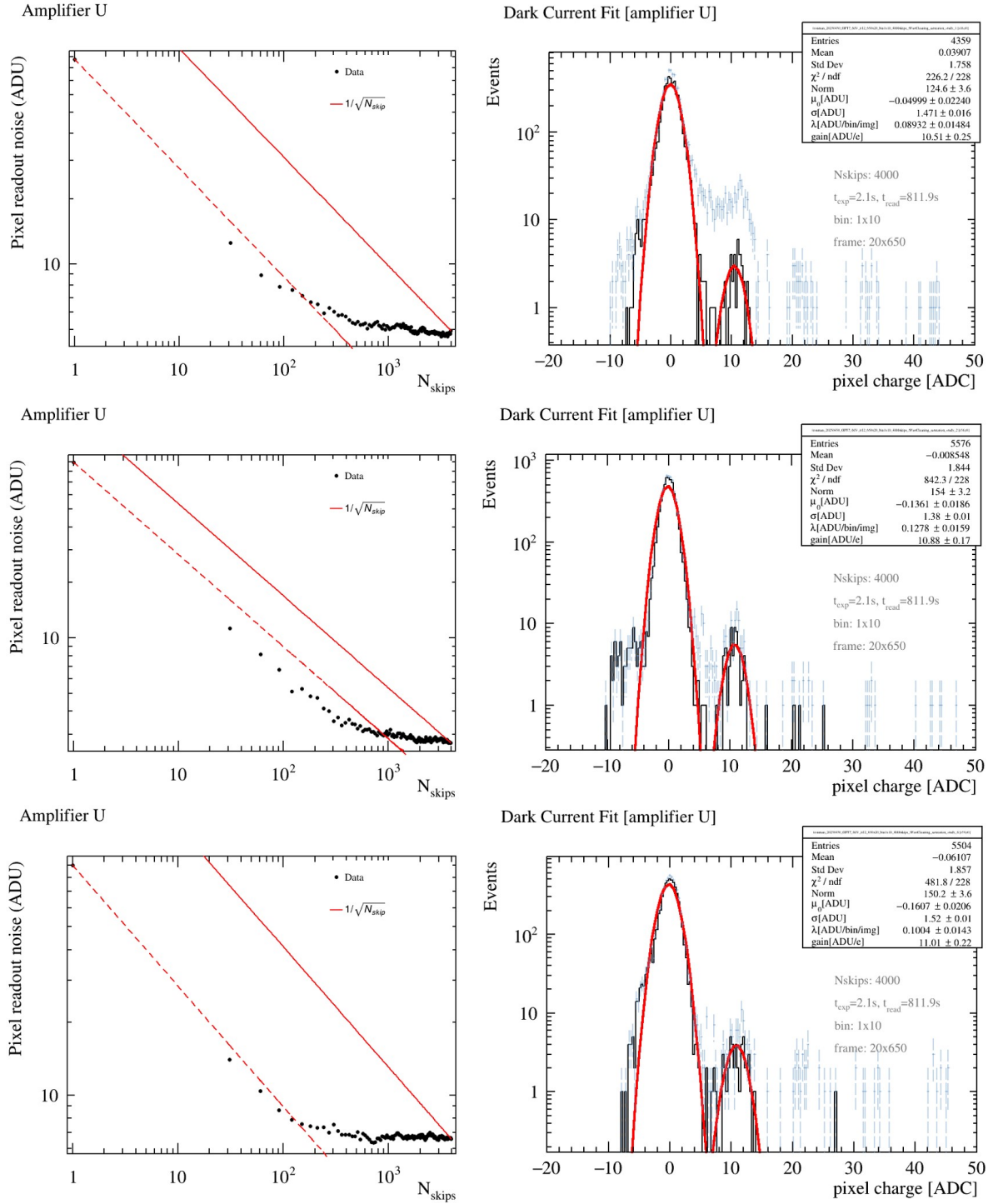


Figure 3.9: Pixel readout noise in ADUs as a function of the number of skips and dark current fit plots for a maximum value of 4000 skips. The images corresponding to these plots have been taken consecutively using the same configuration parameters and taking 5 “cleaning images” in between. The exposure time of the CCD is 2 s.

Chapter 4

Optimization of CCD configuration parameters

An optimization of CCD configuration parameters is key to achieve an efficient charge collection, transfer and readout; which consequently leads to an improvement of the electronic noise. For achieving this purpose, specific relationships [4] between several CCD parameters are required:

- $SW_{hi} > OG_{hi} > V_R$
- $SW_{lo} < OG_{lo} < V_R$
- $V_{drain} < DG_{lo} < V_R < DG_{hi}$
- $RG_{hi} > V_{ref} - V_{eff}$ where $V_{eff} = V_{drain} - SW_{lo}$

where V_R is the reference voltage, TG_{hi} and TG_{lo} are the high and low voltage values of the transfer gate, OG_{hi} and OG_{lo} are the high and low voltage values of the output gate, SW_{hi} and SW_{lo} are the high and low voltage values of the summing well, DG_{hi} and DG_{low} are the high and low voltage values of the dump gate, V_{drain} is the drain voltage and RG_{hi} is the high voltage value of the reset gate. Arbitrary values can be used for both low and high voltage clocks as long as these relationships are fulfilled and the high values remain higher than the lower ones for each of the parameters (e.g. $SW_{hi} > SW_{lo}$). In order to create a potential well with an adequate charge capacity these values need to differ significantly. Otherwise, charge transfer inefficiency (CTI) may occur.

The optimization of the parameters is achieved empirically through the calibration of the dark current and the study of pixel readout noise with guidance from the above relationships. Configuration parameters are shown in Tables 4.1 and 4.2. Black values correspond to parameters that have been kept fixed for all the tests that have been done, while red values refer to parameters that have been varied.

Parameter	High Value [V]	Low Value [V]	Width [μ s]	Overlap Width [μ s]
Horizontal Clocks	[1 , 4.5]	-0.5	[1.25 , 30]	[1.25 , 20]
Vertical Clocks	4.5	1.5	20 , 30	15 , 20
Transfer Gate	4	1.5		
Summing Well	-3	[-10 , -8]	0.24	
Output Gate	-4	-9	0.24	
Dump Gate	-4	-8	0.24	
Reset Gate	5	3	0.24	

Table 4.1: The black values correspond to voltage and timing values that have been kept fixed in all the tests while the red ones refer to values that have been varied for the 6k x 1.5k CCD PP52-U. For the horizontal and vertical clocks, Overlap Width corresponds to the width in time of two gates set at the same low potential value (for instance, it can be graphically seen in the state 2 of Figure 1.2) while Width refers to the width in time of the gate when not overlapping (states 1, 3 and 7 of Figure 1.2).

Parameter	Voltage [V]	Time [μ s]
Pedestal wait time		2.5 , 3
Signal wait time		2.5 , 3
Integration time		[5 , 20]
V_R	-7	
V_{dd}	-19	
V_{drain}	-22	
V_{sub}	45 , 60	

Table 4.2: The black values correspond to voltage and timing values that have been kept fixed in all the tests while the red ones refer to values that have been varied for the 6k x 1.5k CCD PP52-U. The pedestal wait time is the wait time before pedestal integration begins whereas the signal wait time corresponds to the wait time before signal integration begins. V_{sub} is the bias voltage, V_R the reference voltage, V_{dd} the amplifier voltage and V_{drain} the drain voltage.

Non-skip images have been taken with the format 6500 x 1700 (columns x rows) and binning 1 x 1. Skip images have been typically taken with 650 columns, rows in the range of 40 to 200, a x 10 parallel binning (for a ten times faster readout), an integration time of 12 μ s and skips in the range between 1000 and 4000. For instance, an 650 x 100 image with 3000 skips and a 10 x 1 binning takes approximately 50 minutes. A non-skip 6500 x 1700 image with an integration time of 12 μ s takes approximately 5 minutes.

A fine scanning process has been carried out, which involved doing an extensive investigation of how the pixel readout noise and the dark current are impacted for different combinations of parameters within the ranges shown in Tables 4.1 and 4.2. The results show that both are significantly influenced by the integration time and the high voltages of the horizontal clocks, among the varied parameters. The best achieved combination of CCD configuration parameters¹ (i.e. the ones that ensure the most efficient charge collection, transfer and readout) are presented in Tables 4.3 and 4.4. The integration time and the substrate voltage V_{sub} parameters are not included in these tables. As for the integration time, the reason of its exclusion relies on the fact that different optimum values have been obtained for skip and non-skip images. More information is provided in section 4.3. As for the substrate voltage, a value of 40 V is sufficient to fully deplete the CCD [21]. Therefore, CCD images are not really affected by the value of this parameter as long as it is higher than 40 V. Images have been typically taken with 60 V as the substrate voltage value.

¹The CCD configuration file that includes these parameters is shown in the appendix section B.

Parameter	High Value [V]	Low Value [V]	Width [μ s]	Overlap Width [μ s]
Horizontal Clocks	2	-0.5	1.25	1.25
Vertical Clocks	4.5	1.5	30	20
Transfer Gate	4	1.5		
Summing Well	-3	-10	0.24	
Output Gate	-4	-9	0.24	
Dump Gate	-4	-8	0.24	
Reset Gate	5	3	0.24	

Table 4.3: Optimum voltage and timing values for the 6k x 1.5k CCD PP52-U. For the horizontal and vertical clocks, Overlap Width corresponds to the width in time of two gates set at the same low potential value (for instance, it can be graphically seen in the state 2 of Figure 1.2) while Width refers to the width in time of the gate when not overlapping (states 1, 3 and 7 of Figure 1.2).

Parameter	Voltage [V]	Time [μ s]
Pedestal wait time		2.5
Signal wait time		2.5
V_R	-7	
V_{dd}	-19	
V_{drain}	-22	

Table 4.4: Optimum voltage and timing values for the 6k x 1.5k CCD PP52-U. The pedestal wait time is the wait time before pedestal integration begins whereas the signal wait time corresponds to the wait time before signal integration begins. V_R is the reference voltage, V_{dd} the amplifier voltage and V_{drain} the drain voltage.

In the following sections, a detailed description is provided for the optimization of SW_{lo} , H_{hi} , and the integration time.

4.1 Low voltage value of the summing well

The parameter SW_{lo} was varied within the range of -8 V to -10 V. Taking into account the fifth relationship shown at the beginning of the chapter and given that $V_R = -7$ V and $OG_{lo} = -9$ V, the optimal value of SW_{lo} should be lower than -9 V. Hence, it was expected that a value of $SW_{lo} = -10$ V would provide better results compared to -9 V or -8 V. However, contrary to expectations, similar values of dark current and pixel readout noise were obtained for SW_{lo} set at -8 V, -9 V, and -10 V, as shown in Table 4.5.

SW_{lo} [V]	$\lambda \pm \Delta\lambda$ [ADU/bin/img]	$\sigma \pm \Delta\sigma$ [ADU]
-8	0.021 ± 0.006	1.241 ± 0.006
-9	0.020 ± 0.004	1.26 ± 0.03
-10	0.020 ± 0.003	1.219 ± 0.016

Table 4.5: Dark current (λ) and pixel readout noise (σ) values for the 6k x 1.5k CCD PP52-U at different SW_{lo} settings (-8 V, -9 V, and -10 V). Each value of λ and σ is an average calculated from five measurements. The error of these two magnitudes represent the standard deviation of the five measurements respectively.

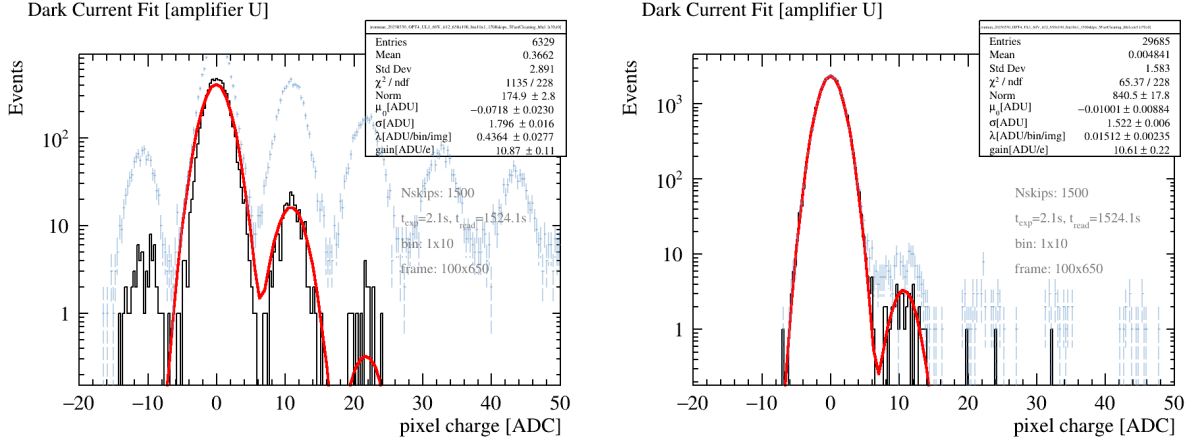
The results presented in Table 4.5 indicate that the values of λ remain consistent for the different SW_{lo} values, while σ is slightly lower for $SW_{lo} = -10$ V. However, it was expected that a pronounced difference would be observed in both σ and λ values, since if both SW_{lo} and OG_{lo} are set to the same value or if SW_{lo} is higher than OG_{lo} , charge should be transferred inefficiently from the sense node to the summing well. The correct charge transfer between these gates is illustrated in Figure 1.11 at the introduction subsection 1.3.1, where it can be seen that the low voltage value of the SW is lower than the low voltage value of the OG. An incorrect charge transfer should adversely affect the pedestal calculation, which is done when charge is at the SW, and charge calculation, which is done when charge is at the SN.

In the LBC and other CCD experimental setups at the collaborating universities, the optimization of parameters has demonstrated that setting both SW_{lo} and OG_{lo} to -9 V provides better results, despite contradicting the relationship that states that SW_{lo} should be lower than OG_{lo} . Likewise, when reading only the CCD serial register, the IFCA setup exhibits good results with both potentials set at -9 V. Further investigation on this topic is required, including the understanding of the case where $SW_{lo} = -8$ V. Therefore, additional experiments and analysis should be conducted to understand the effect of different SW_{lo} values on the measured noise and dark current in these scenarios.

4.2 High voltage value of horizontal clocks

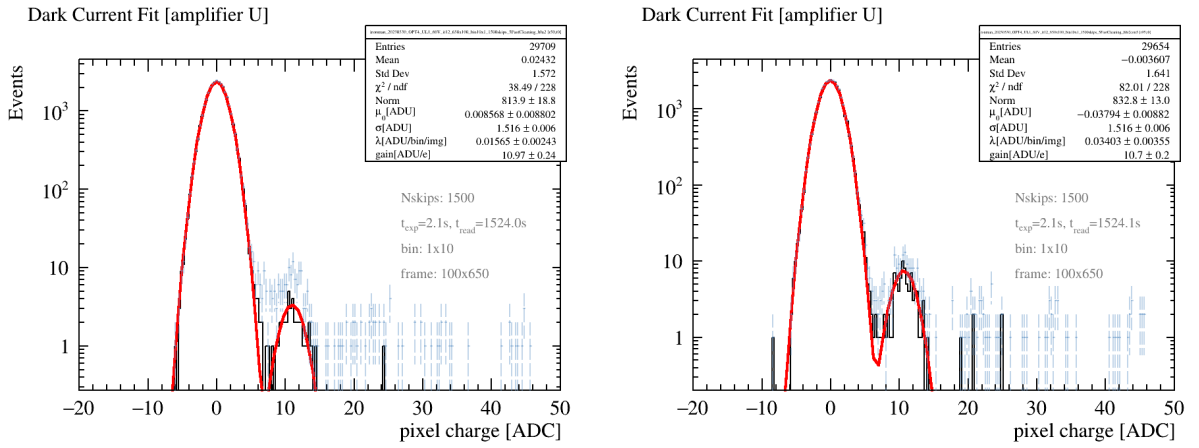
The high voltage value of horizontal clocks H_{hi} has been varied in a range between 1 to 4.5 V. Finding the optimal value for the CCD PP52-U relies on experimental investigations.

In Figures 4.1 and 4.2 the dark current fit plots are shown while in Figure 4.3 the readout noise in ADUs is depicted as a function of the number of skips. The provided figures clearly demonstrate that noise saturates at a certain number of skips, as illustrated in 4.3g and 4.3h, and that there is a notable increase in the measured charge when H_{hi} is set to 4 V or 4.5 V, as can be seen in 4.2c and 4.2d. It is important to note that for $H_{hi} = 1.0$ V the potential difference between the low, which has been set at -0.5 V, and high value is not enough to properly collect the charge. Consequently, it adversely affects the charge transfer process and the charge readout, resulting in a higher measured charge, as depicted in 4.1a, and in a non-linear behaviour of the pixel readout noise as a function of the number of skips, as can be seen in 4.3a. The value of $H_{hi} = 2.0$ V has been selected as the optimal value, as it provides the lowest combination of σ and λ values. However, it is worth noting that H_{hi} values of 1.5 V and 2.5 V also provides good results, exhibiting a high degree of similarity to those obtained with 2.0 V. Consequently, these alternative values could be also be employed and still deliver satisfactory results.



(a) Dark current fit plot of an image taken with $H_{hi} = 1.0$ V. The noise is $\sigma = (1.796 \pm 0.016)$ ADU and the dark current rate is $\lambda = (0.44 \pm 0.03)$ ADU/bin/img.

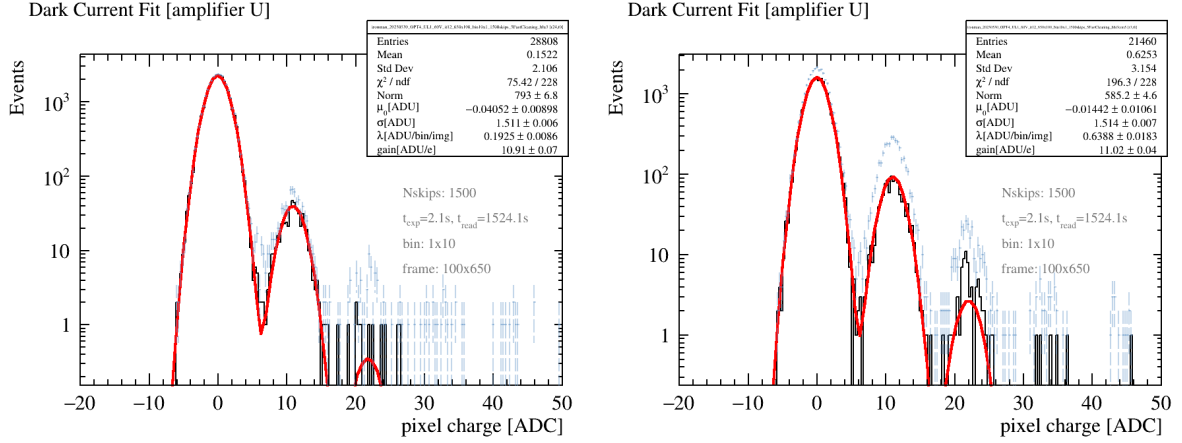
(b) Dark current fit plot of an image taken with $H_{hi} = 1.5$ V. The noise is $\sigma = (1.522 \pm 0.006)$ ADU and the dark current rate is $\lambda = (0.015 \pm 0.002)$ ADU/bin/img.



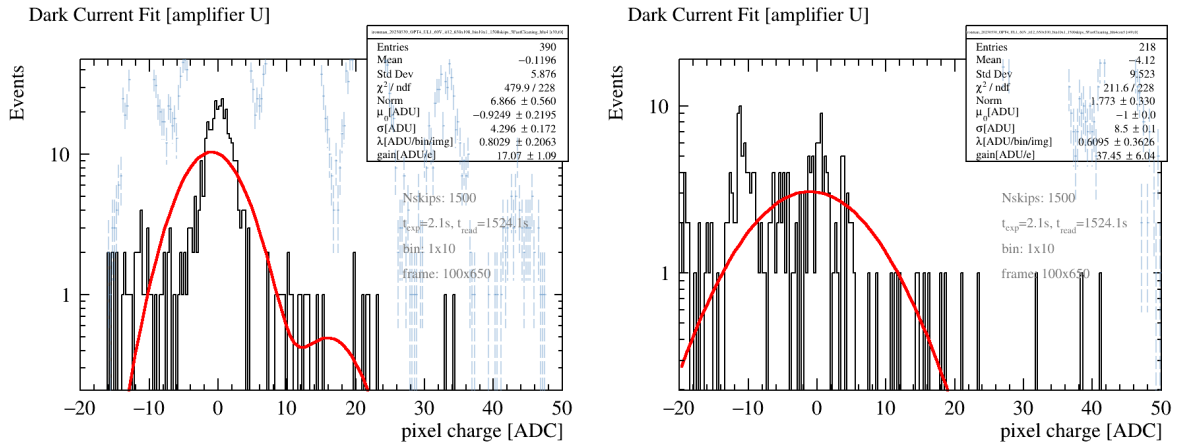
(c) Dark current fit plot of an image taken with $H_{hi} = 2.0$ V. The noise is $\sigma = (1.516 \pm 0.006)$ ADU and the dark current rate is $\lambda = (0.016 \pm 0.002)$ ADU/bin/img.

(d) Dark current fit plot of an image taken with $H_{hi} = 2.5$ V. The noise is $\sigma = (1.516 \pm 0.006)$ ADU and the dark current rate is $\lambda = (0.034 \pm 0.004)$ ADU/bin/img.

Figure 4.1: Dark current fit plots for images taken changing the parameter H_{hi} in a range between 1.0 V and 2.5 V in steps of 0.5 V. The exposure time of the CCD is 2 s.



(a) Dark current fit plot of an image taken with $H_{hi} = 3.0$ V. The noise is $\sigma = (1.511 \pm 0.006)$ ADU and the dark current rate is $\lambda = (0.193 \pm 0.009)$ ADU/bin/img. (b) Dark current fit plot of an image taken with $H_{hi} = 3.5$ V. The noise is $\sigma = (1.514 \pm 0.007)$ ADU and the dark current rate is $\lambda = (0.639 \pm 0.018)$ ADU/bin/img.



(c) Dark current fit plot of an image taken with $H_{hi} = 4.0$ V. The measured charge is too high to accurately perform a dark current fit. Consequently, σ and λ can not be properly obtained. (d) Dark current fit plot of an image taken with $H_{hi} = 4.5$ V. The measured charge is too high to accurately perform a dark current fit. Consequently, σ and λ can not be properly obtained.

Figure 4.2: Dark current fit plots for images taken changing the parameter H_{hi} in a range between 3.0 V and 4.5 V in steps of 0.5 V. The exposure time of the CCD is 2 s.

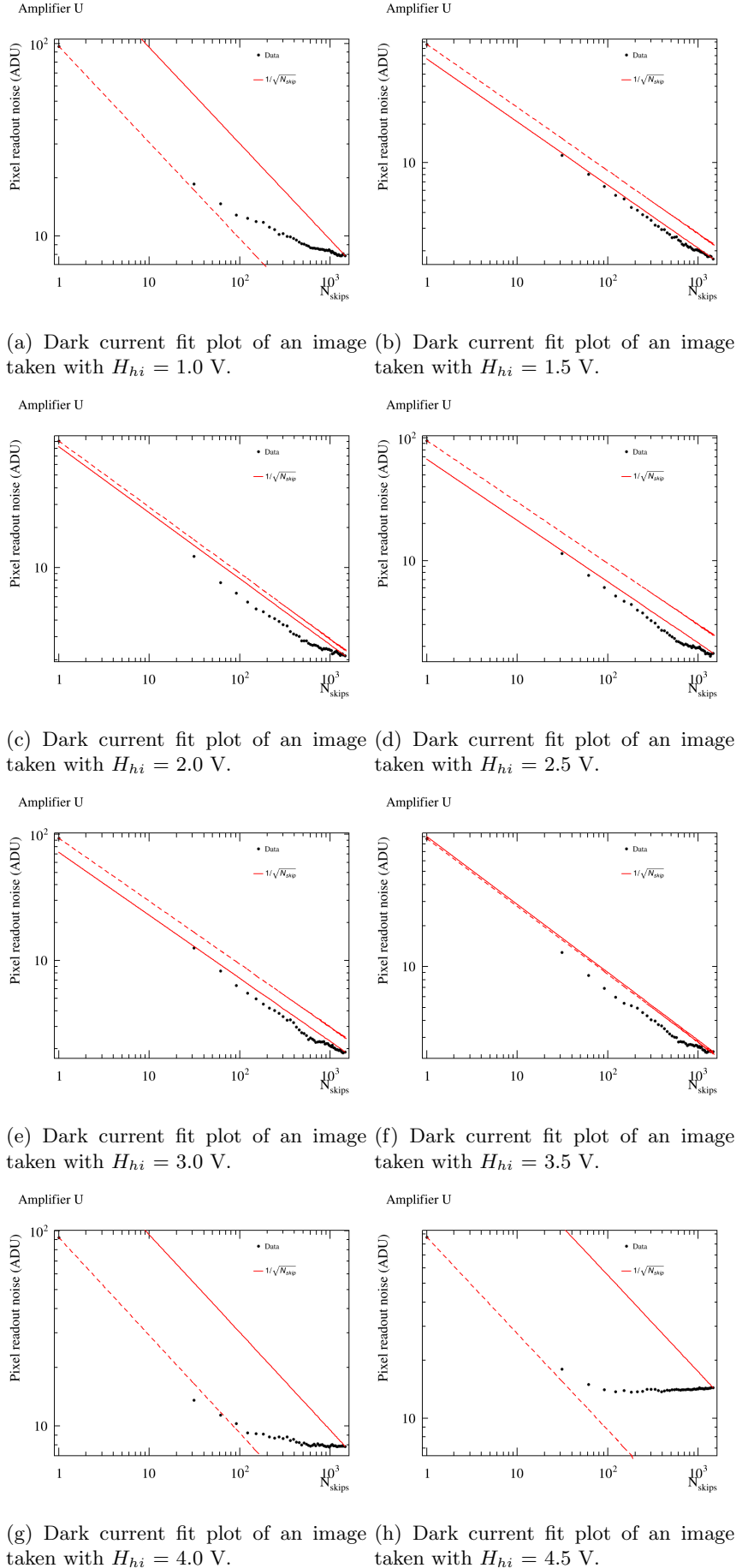


Figure 4.3: Pixel readout noise as a function of the number of skips for images taken changing the parameter H_{hi} in a range between 1.0 V and 4.5 V in steps of 0.5 V. The exposure time of the CCD is 2 s.

4.3 Integration time

The study presented in Chapter 3 was conducted before achieving the optimized configuration parameters. When the process of parameter optimization was started, the influence of the electromagnetic noise on the CCD images was discovered. Consequently, the plot depicting the relationship between the pixel readout noise and integration time, shown in Figure 3.8, does not have the optimized configuration parameters. Therefore, this plot has been reproduced for the skipper case with the best configuration parameters achieved.

In Figure 4.4, the blue dots represent the pixel readout noise as a function of the integration time obtained using the optimized configuration parameters. Most of the points of this curve remain lower than the points from other curves obtained with non-optimized parameters. Ideally, it would be expected for all the points to remain below, but for lower values of the integration time, the noise highly fluctuates. The values of the noise in the range of approximately 19 μs to 23 μs are the lowest, and consequently the optimal ones. However, choosing higher integration times for reading CCD images results in longer CCD image acquisition times. To achieve a balance between reducing image acquisition time and maintaining low noise levels, images are typically taken with an integration time of 12 μs . This value is sufficiently long to avoid the observed noise fluctuations at lower integration times and provides good noise results.

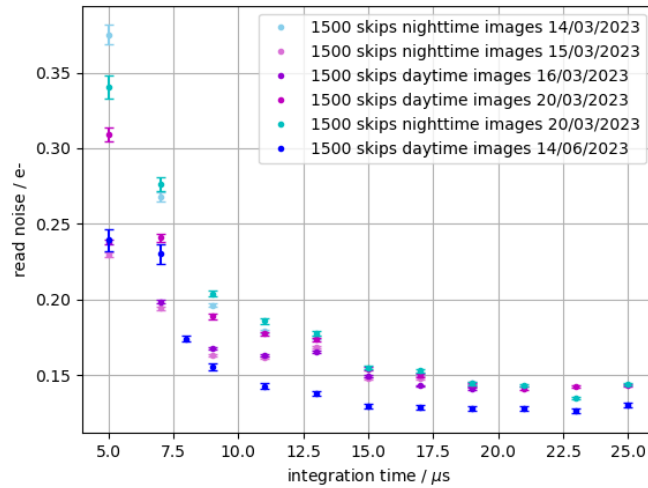


Figure 4.4: Read noise as a function of the integration time for 1500 skips images taken with the optimal configuration parameters achieved.

Chapter 5

Study of silicon defects as a function of temperature

This study aims to investigate the effects of temperature on CCD PP52-U silicon defects, focusing on the formation and characteristics of hot columns and hot pixels, i.e. regions where intrinsic dark current is higher due to traps generated by lattice defects. Therefore, the temperature has been varied from 120 K to 230 K in steps of 10 K. For each temperature, 50 non-skip 6500 x 1700 images have been taken with an integration time of 12 μ s, a substrate voltage at 60 V, the operation parameters of Tables 4.1 and 4.2, an exposure time of 60 seconds and taking a few “cleaning images” between each of the images. To obtain pedestal subtracted images, these images have been reprocessed using the analysis software Waders (A.2). Then, an average image was generated by combining the 50 reprocessed images, using python (see D), for each of the temperatures to enhance statistically the effects of the silicon defects. These images have been further analyzed using the [analysis software ROOT¹](#).

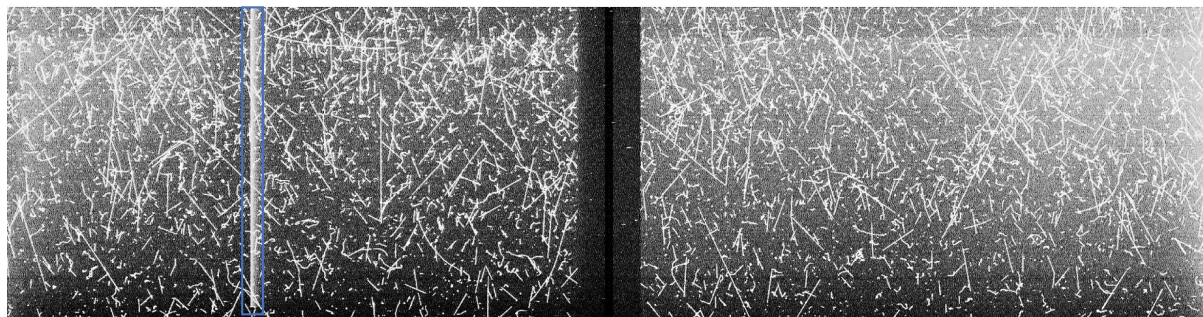
The appearance of hot columns and super-hot pixels on the images has been initially observed using DS9 and ROOT at a temperature of 180 K. As a result, this study has focused on the temperature range between 180 and 230 K, the average images obtained for each of the temperatures are shown in Figures 5.1 and 5.2. All the white tracks that have not been framed correspond to ionization tracks from different particles.

At a temperature of 180 K only one hot column (framed by a blue rectangle) caused by a super-hot pixel appears on the left side of the image. A high difference between this image and the one corresponding to 190 K can be seen in Figure 5.1, since at 190 K five additional hot-columns emerge. To clearly observe the super-hot pixels responsible for the creation of each hot column, a zoom has been performed at the beginning of each of them, as indicated by red rectangles. It is important to note that due to the high number of tracks in the image, a “clean” zoom (i.e. a zoom without ionization tracks) has not been able to be performed and in consequence a few tracks appear in the zoom images. In the image corresponding to 200 K, a new hot column appears as well as a bad column, which has been highlighted with a purple rectangle. Two zooms have been conducted on the left side to the image, as indicated by the red rectangles. The first zoom reveals the initial development of a super-hot pixel at the bottom, leading to a weak hot column that overlaps with the existing one created by the super-hot pixel located above, which has begun to spill over vertically. The second zoom, located further to the right, displays a stronger hot column compared to the same one at 190 K. The blue background color provides better visibility of the beginning of this hot column. It is important to note that there is a ionization track crossing over the hot column, making the beginning of the hot column to appear wider than its actual width. At 210 K, there are no particularly notable changes observed, except for the fact that the super-hot pixel seen in the zoomed-in view on the left has spilled over vertically even further. At 220 K, it can be seen that the super-hot pixel shown in the first zoom to the left has started to spill over vertically. Additionally, the super-hot pixel located in the second zoom (to the right of the previous men-

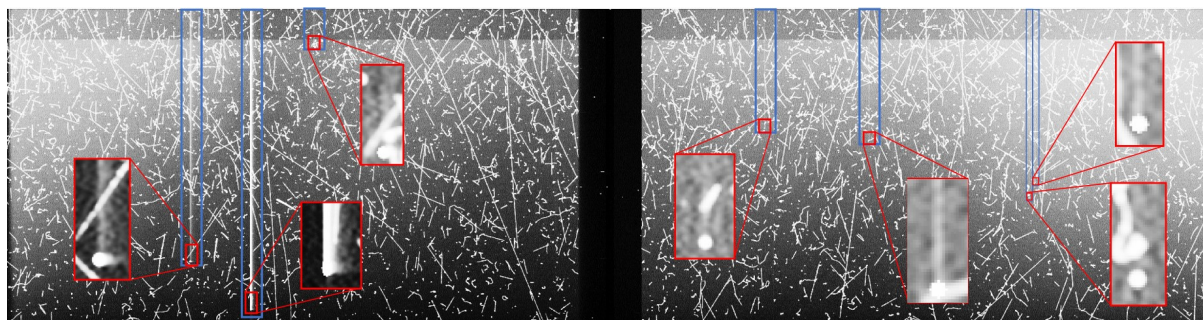
¹See the tutorial from https://root.cern/doc/master/group__tutorial__FITS.html

tioned super hot pixel) has completely spilled over, even reaching the other super-hot pixel located below.

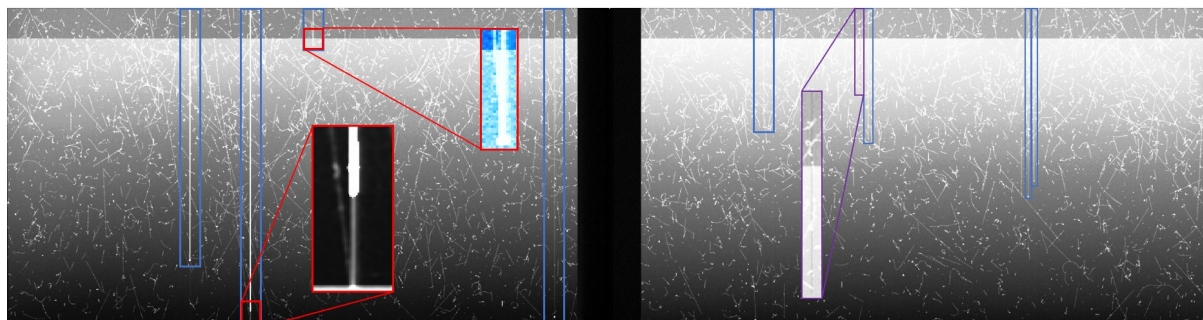
As the temperature increases, the dark current increases too. Therefore, the dark current progressively approaches values closer to the ones of the ionization tracks. Consequently, the ionization tracks are seen less clearly as the temperature increases until they are not longer distinguishable, as can be observed in Figures 5.1 and 5.2.



(a) “DS9” image of the CCD taken at a temperature of 180 K. The only hot column that appears has been framed with a blue rectangle.

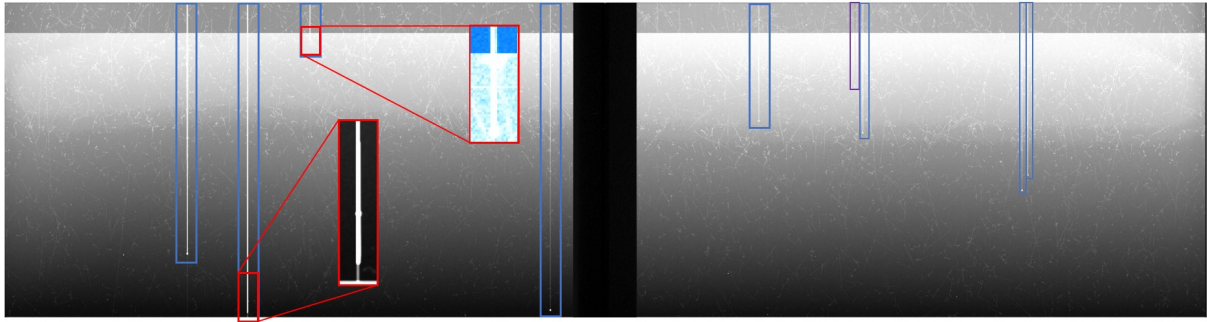


(b) “DS9 image of the CCD taken at a temperature of 190 K. Hot columns have been framed with blue rectangles and a zoom has been done in each of the super hot pixels (red rectangles) that create each of the hot columns.

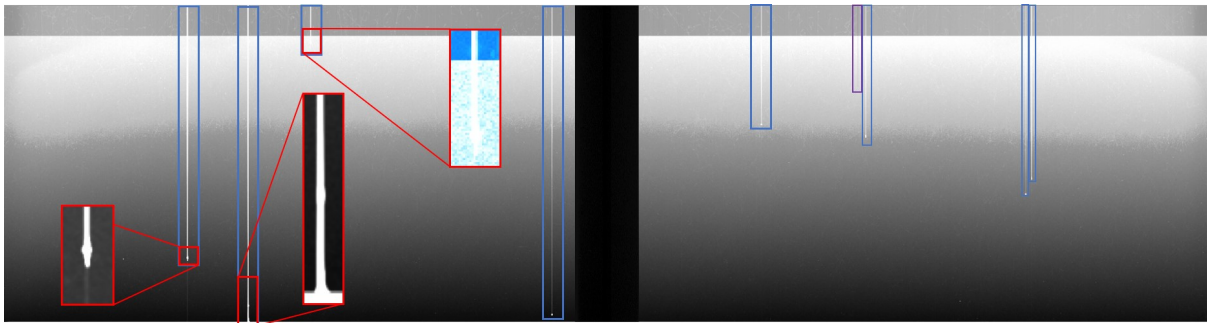


(c) “DS” image of the CCD taken at a temperature of 200 K. Hot columns have been framed with blue rectangles and a bad column has been framed with a purple rectangle. A zoom has been done to two of the super hot pixels.

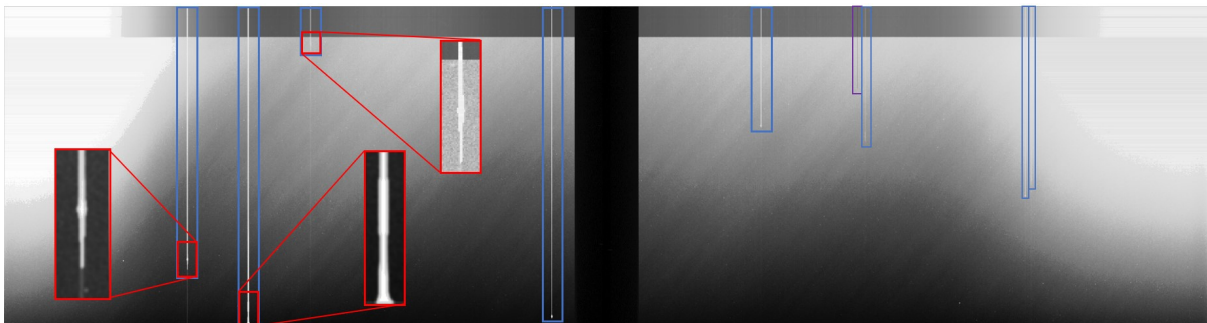
Figure 5.1: “DS9” images of the CCD taken at temperatures of 180, 190 and 200 K.



(a) “DS9” image of the CCD taken at a temperature of 210 K. Hot columns have been framed with blue rectangles and a bad column has been framed with a purple rectangle. A zoom has been done to two of the super hot pixels.



(b) “DS9” image of the CCD taken at a temperature of 220 K. Hot columns have been framed with blue rectangles and a bad column has been framed with a purple rectangle. A zoom has been done to three of the super hot pixels.



(c) “DS9” image of the CCD taken at a temperature of 230 K. Hot columns have been framed with blue rectangles and a bad column has been framed with a purple rectangle. A zoom has been done to three of the super hot pixels.

Figure 5.2: “DS9” images of the CCD taken at temperatures of 210, 220 and 230 K.

In the data obtained from the LBC at 120 K, it was observed that hot columns exhibited an exponential behavior. To investigate whether this behavior also applies to the CCD PP52-U, hot columns have been analyzed using the analysis software ROOT. In particular, the behaviour of the hot-column that starts appearing at 180 K has been studied at different temperatures. It is worth noting that as the temperature increases, this column undergoes a transition from exhibiting an exponential decay pattern to a “Gaussian” like distribution, as illustrated in Figures 5.3 and 5.4. The other hot-columns that appear at higher temperatures seem to exhibit a “Gaussian” like distribution since the beginning of their appearance. Therefore, based on what was seen at the LBC, SNOLAB and the IRONMAN setup, it seems that for lower temperatures the pixels of the hot-columns present charge transfer inefficiency, leading to the appearance of the exponential behaviour. At higher temperatures, the hot-columns present a

higher amount of charge and consequently the diffusion of the charge from these pixels is bigger, leading to the appearance of the “Gaussian” like distribution.

Further investigation on this topic requires employing other CCDs that exhibit hot-columns at low temperatures to check if this behaviour occurs. Moreover, to confirm the ”Gaussian” like behaviour at higher temperatures it could be requested to the DAMIC-M collaboration to take images at higher temperatures in the LBC.

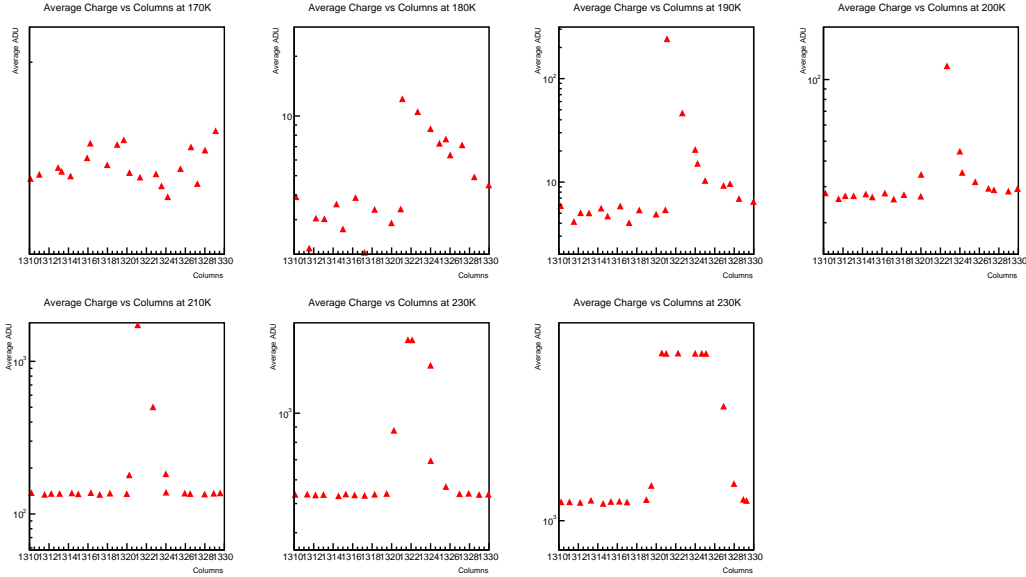


Figure 5.3: These plots represent the average charge in ADUs of each of the columns as a function of the column number. The evolution of the hot-column that is first seen at a temperature of 180 K (see 5.1a) is shown in a range from 180 K to 230 K. Notice that at 170 K this hot-column is still not present.

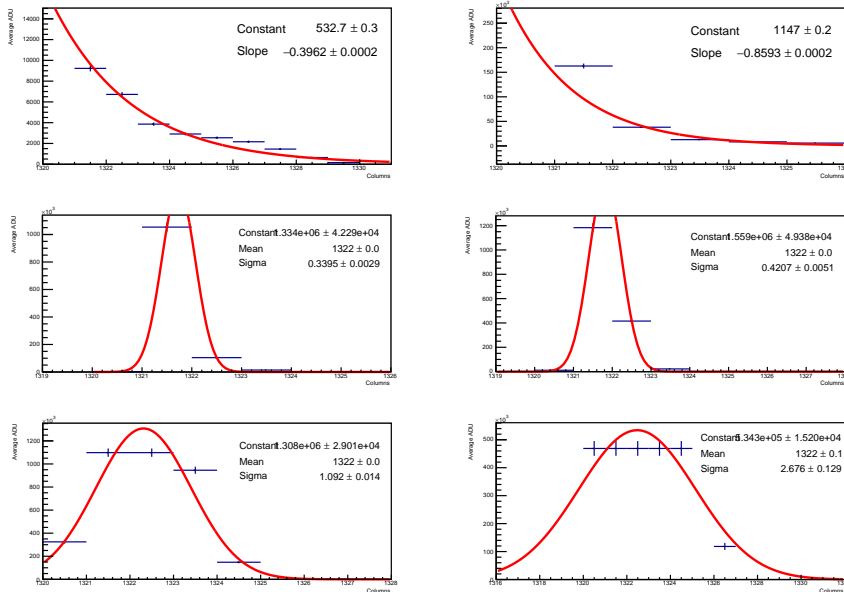


Figure 5.4: These plots depict the fitting of the data from the plots of Figure 5.3. In the first and second plots the fitting of the data corresponds to an exponential fit while in the rest of the plots the fitting is Gaussian fit. These fittings have been performed only for qualitative purposes.

Chapter 6

Conclusions

The commissioning of the CCD experimental setup (IRONMAN) has been done in this project for the first time. This experimental setup is located in a cleanroom at IFCA. Specifically, the commissioning efforts have focused on characterizing a non-scientific Charge Couple Device (CCD), named CCD PP52-U, which incorporates a skipper readout system.

To effectively characterize this CCD experimental setup, I have needed to acquire a comprehensive understanding on how CCDs work and familiarize myself with the startup and data acquisition procedures specific to this CCD setup. Throughout the course of this project, I have taken a total of 5634 images in a range of temperatures from 120 K to 230 K to achieve the specific objectives of the research. These objectives involve investigating the impact of electromagnetic noise on CCD images, optimizing the CCD configuration parameters for the skipper readout system and studying the influence of temperature on silicon defects through trap manifestations as hot columns, bad columns, super-hot pixels, etc. For viewing the images, I have needed to learn how the DS9 software tool works (see A.1). Specifically, skipper images need to be first reprocessed before being visualized with DS9. Therefore, I have reprocessed them with WADERS analysis software (see A.2), which I have installed through a docker image¹. I have also used bash (see C.2.1) and python (see D) programming languages as well as ROOT to do several of the analysis shown in this work.

The optimization of the CCD configuration parameters, among the varied ones, has focused on the integration time, the low voltage value of the summing well and the high voltage values of the horizontal clocks. This optimization process plays a crucial role in improving the performance of the CCD, ensuring accurate measurements and reducing unwanted noise contributions. Through the examination of the impact on pixel readout noise and dark current, the parameter values that provide the best performance of the CCD have been determined. These optimized parameter values can be found in Tables 4.1 and 4.2. During the optimization process, it was found that the IFCA setup is highly sensitive to electromagnetic noise. Various electromagnetic noise sources have been found to affect CCD images, including the operation of the experimental setup in the adjacent clean room and an insufficient isolation of multiple wires responsible for controlling electronic instruments within the CCD setup. Additionally, an intermittent noise of unknown origin has been identified. Differentiating between them is essential for determining the validity of the data extracted from the images, such as the pixel readout noise.

Furthermore, this study has focused on investigating various manifestations of traps generated by silicon defects in relation to the temperature. As the temperature is raised, the evident and expected increase in the occurrence of these trap manifestations, such as bad columns, super-hot pixels, and hot columns, has been observed. Specifically, a study of the changing behaviour of the hot columns as a function of the temperature has been carried out. In general this study provides valuable insights into the adverse behavior of the CCD at temperatures in the range from 180 K to 230 K.

Overall, this project provides information about the impact of electromagnetic noise, the optimiza-

¹<https://www.docker.com/>

tion of CCD configuration parameters, and the influence of temperature on traps manifestations. These findings are crucial for improving the image quality, reducing noise and determining whether the acquired images are reliable or need to be discarded due to being affected by electromagnetic noise.

It can be concluded that the IRONMAN setup works successfully and that it can be used for characterizing CCDs of future experiments (DAMIC-M and Oscura).

6.1 Future work

This work opens a new line of research in the field of electromagnetic noise in the system. Several recommendations can be made based on the findings of this study. Firstly, it is suggested to design a better grounding system. This can involve studying the electrical power input in the laboratory and the utilization of an Uninterruptible Power Supply (UPS) to mitigate any power grid instabilities that may contribute to the noise. The recent acquisition of the “bias” board will replace the three external power sources that are currently being used. This replacement is expected to reduce the electromagnetic noise.

Moreover, further investigation is necessary to address uncertainties related to the optimization of the summing well. The theoretical relationships, including the one related to the uncertainties in the optimization of the summing well, need to be studied in more detailed and validated through experimental measurements in which higher amounts of charge are read. For reading more charge, it is necessary to take images in which the CCD’s active region is read.

Additionally, a new alternative reading system has been recently purchased, specifically designed for skipper CCDs, called Low Threshold Acquisition (LTA). This system is expected to reduce noise and improve the overall performance in the CCD operation.

Furthermore, investigations of the hot-columns at different temperatures should be pursued to confirm the distinct behaviours observed and the charge transfer inefficiency and diffusion hypothesis.

Bibliography

- [1] “Dark matter,” CERN. (May 26, 2023), [Online]. Available: <https://home.cern/science/physics/dark-matter>.
- [2] J. Zavala and C. S. Frenk, “Dark matter haloes and subhaloes,” *Galaxies*, vol. 7, no. 4, p. 81, 2019. DOI: [10.3390/galaxies7040081](https://doi.org/10.3390/galaxies7040081).
- [3] “Dark matter hub,” Interactions. (Dec. 12, 2022), [Online]. Available: <https://www.interactions.org/node/13234>.
- [4] M. Traina, “Search for light dark matter and exploration of the hidden sector with the damic at snolab and damic-m charge-coupled devices,” Thèse de doctorat dirigée par Letessier-Selvon, Antoine Physique de l’Univers Sorbonne université 2022, Ph.D. dissertation, 2022. [Online]. Available: <http://www.theses.fr/2022S0RUS307/document>.
- [5] “DAMIC: Dark matter in ccds,” DAMIC @ UW. (), [Online]. Available: <https://www.npl.washington.edu/damic/description>.
- [6] M. Traina. “Results on low-mass weakly interacting massive particles from a 11 kg d target exposure of DAMIC at SNOLAB (ICRC2021 Proceedings),” arXiv.org. (2021), [Online]. Available: <https://arxiv.org/abs/2108.05983>.
- [7] A. Aguilar-Arevalo *et al.*, “Confirmation of the spectral excess in DAMIC at SNOLAB with skipper CCDs,” Jun. 2023. arXiv: [2306.01717](https://arxiv.org/abs/2306.01717) [[astro-ph.CO](https://arxiv.org/abs/2306.01717)].
- [8] “DAMIC-M: Dark matter in ccds at modane,” DAMIC-M. (), [Online]. Available: <https://damic.uchicago.edu/>.
- [9] I. Arnquist, N. Avalos, P. Bailly, *et al.*, “The DAMIC-M experiment: Status and first results,” Nov. 2022. arXiv: [2210.12070](https://arxiv.org/abs/2210.12070) [[physics.ins-det](https://arxiv.org/abs/2210.12070)]. [Online]. Available: <https://arxiv.org/abs/2210.12070>.
- [10] “The nobel prize in physics 2009.” (), [Online]. Available: <https://www.nobelprize.org/prizes/physics/2009/summary/>.
- [11] K. Ramanathan, “Particles taking selfies: Investigations into light dark matter using silicon charge coupled devices,” Ph.D. dissertation, University of Chicago, 2020. [Online]. Available: <https://doi.org/10.6082/uchicago.3632>.
- [12] J. Zhou, “Direct dark matter detection with the DAMIC experiment at SNOLAB,” Ph.D. dissertation, University of Chicago, 2015. DOI: [10.6082/M1V985ZB](https://doi.org/10.6082/M1V985ZB).
- [13] M. F. Sofo Haro, “Sensores multipixel ccd de ultra bajo ruido de lectura para detección de partículas,” Ph.D. dissertation, Universidad Nacional de Cuyo, 2017. [Online]. Available: <http://labdpr.cab.cnea.gov.ar/student/doctorado-sofo.pdf>.
- [14] G. Knoll, *Radiation Detection and Measurement*. Wiley, 2010, ISBN: 9780470131480. [Online]. Available: <https://books.google.fr/books?id=4vTJ7UDel5IC>.
- [15] J. R. Janesick, T. S. Elliott, A. Dingiziam, *et al.*, “New advancements in charge-coupled device technology: subelectron noise and 4096 x 4096 pixel CCDs,” in *Charge-Coupled Devices and Solid State Optical Sensors*, M. M. Blouke, Ed., International Society for Optics and Photonics, vol. 1242, SPIE, 1990, pp. 223–237. DOI: [10.1117/12.19452](https://doi.org/10.1117/12.19452). [Online]. Available: <https://doi.org/10.1117/12.19452>.

-
- [16] J. Tiffenberg. “Counting electrons with the skipper-ccd,” Fermi National Laboratory. (2020), [Online]. Available: https://indico.fnal.gov/event/23109/contributions/193269/attachments/132888/163601/ura_eca.pdf.
- [17] A. Y. Matalon, “Searching for light dark matter with damic at snolab and damic-m: Investigations into radioactive backgrounds and silicon skipper charge-coupled devices,” Ph.D. dissertation, University of Chicago, 2021. [Online]. Available: <https://doi.org/10.6082/uchicago.3632>.
- [18] M. Moll. “Defects in silicon crystals - cern.” (Nov. 2004), [Online]. Available: <https://www.yumpu.com/en/document/view/18917938/defects-in-silicon-crystals-cern> (visited on 06/04/2023).
- [19] F. Jansen. “Basics of ccds and astronomical imaging.” (2014), [Online]. Available: https://www.public.asu.edu/~rjansen/ast598/ast598_jansen2014.pdf (visited on 06/04/2023).
- [20] A. Aguilar-Arevalo *et al.*, “DAMIC at SNOLAB,” *Physics Procedia*, vol. 61, pp. 21–33, 2015, 13th International Conference on Topics in Astroparticle and Underground Physics, TAUP 2013, ISSN: 1875-3892. DOI: <https://doi.org/10.1016/j.phpro.2014.12.006>. [Online]. Available: <https://www.sciencedirect.com/science/article/pii/S1875389214006191>.
- [21] S. E. Holland, D. E. Groom, N. P. Palaio, R. J. Stover, and M. Wei, “Fully depleted, back-illuminated charge-coupled devices fabricated on high-resistivity silicon,” *IEEE Transactions on Electron Devices*, vol. 50, no. 1, pp. 225–238, 2003.
- [22] C. De Dominicis, “Search for light dark matter with damic-m experiment,” Thèse de doctorat dirigée par Settimo, Mariangela Physique Subatomique et Instrumentation Nucléaire Ecole nationale supérieure Mines-Télécom Atlantique Bretagne Pays de la Loire 2022, Ph.D. dissertation, 2022. [Online]. Available: <http://www.theses.fr/2022IMTA0313/document>.
- [23] N. Castelló-Mor. “Documentation for pysimdamicm package - waders 5.3.1 documentation.” (s.f.), [Online]. Available: <https://ncastell.web.cern.ch/ncastell/pysimdamicm/index.html>.

Appendix A

Analysis software

A.1 SAOImage DS9

SAOImage DS9 (also known as DS9) is an imaging and data visualization software widely used. This software tool offers a range of features that enables the analysis of CCD images. FITS (Flexible picture Transport System) is one of the several picture formats that it supports.

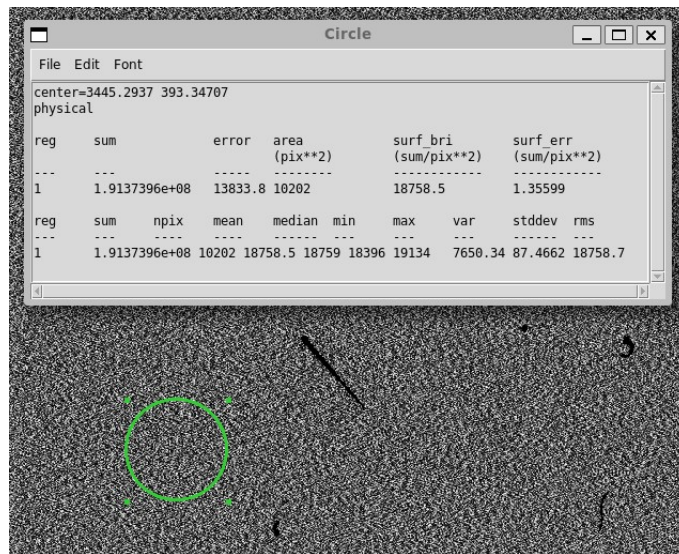


Figure A.1: Example of DS9 analysis capabilities. The pixel area inside the green circle (ROI) is characterized.

DS9 offers features that allow users to zoom, pan, and scale images for an in-depth analysis. Additionally, it enables the definition and manipulation of regions of interest (ROIs) on the images, allowing the measurement of parameters like the mean, median, and standard deviation within these specific regions. In the context of the Gaussian PVD hypothesis, the mean and median provide an estimation of the pedestal or no-charge pixel value and the standard deviation corresponds to the readout noise in ADUs. Figure A.1 shows an example of DS9 analysis capabilities.

Non-skip “raw” images can be visualized and analyzed with this software tool but skip-images require a specific processing prior to being visualized using DS9. This processing technique is not available in DS9, so an alternative software is needed for the processing and analysis of skipper images (see A.2).

A.2 WADERS

WADERS (softWARE for Dark matter ExpeRiments with Skipppers) is a Python3 based code used to process both simulations and real data [22]. With this software non-skip and skip images can be correctly processed and analyzed.

This software incorporates a library of processes (e.g. `CompressSkipperProcess`, `PedestalSubtractionProcess`, etc.), in other words, a collection of predefined algorithms to process the data. Each of the processes can be either activated or de-activated as well as configured at runtime by the user through a JSON file.

The following is an overview of each of the processes included in the JSON file. `CompressSkipperProcess` is a process that combines all single skip images into a single image. This process can be configured to generate two images, in the first one the value of each pixel corresponds to the mean value, calculated using all the skipper images taken, while on the second one the value of each pixel corresponds to the standard deviation, i.e. the readout noise. The `PedestalSubtractionProcess` estimates the pedestal of the image and subtracts it, resulting in a pedestal-subtracted image. The `RNvsNskipsPlot` process provides a plot of the readout noise in ADUs as a function of the number of skips. To accurately quantify the dark current, it is important to accurately identify and remove clusters. The `ClusterFinder` process performs a systematic search of the image, looking for pixels above a clustering threshold. Any contiguous group of pixels with charge above this threshold is considered a potential cluster. If at least one pixel within that region exceeds another defined limit (above the threshold), that region is considered a cluster. The `BuildClusterMask` process then masks all the pixels that fulfill the second condition. The dark current can be quantified by applying a Gaussian-Poisson convolution to the “de-clustered” histogram using the `FitDarkCurrentProcess`. This process provides values for parameters such as the readout noise (σ) in ADUs, the dark current rate (λ) in ADUs per bin per image, and the gain (ADUs per e^-). The `ChargeLossPlot` process generates a set of plots to study charge loss between skips. Noise spectral decomposition is a valuable diagnostic tool for identifying and potentially mitigating electronic noise sources. The `FFTNoisePlot` process generates plots of the Fast Fourier Transform of a skipper image, allowing for the analysis of noise in skips and pixels. Further information can be found at [23].

Example of a JSON file:

```

1 {
2   "input":
3   {
4     "image":
5     {
6       "extensions" : 0,
7       "skip_image" : true,
8       "axis_to_compress" : 1,
9       "correct_leach_bug" : true,
10      "correct_polarity" : true,
11      "id_skip_start" : 40,
12      "id_skip_end" : -1,
13      "id_row_start" : 0,
14      "id_row_end" : -1,
15      "id_col_start" : 0,
16      "id_col_end" : -1,
17      "n_rows_prescan" : 0,
18      "n_rows_overscan" : 0,
19      "ccd_rows" : 1548,
20      "n_cols_prescan" : 8,

```

```
21     "ccd_cols" : 6144,
22     "n_amp" : 2,
23     "save_image" : true
24 },
25 "datetime":
26 {
27     "exposure_start" : "EXPSTART",
28     "readout_start" : "RDSTRT",
29     "readout_end" : "RDEND"
30 },
31 "scp":
32 {
33 },
34 "convention":
35 {
36     "ampdir" : "VCKDIRN",
37     "itgtime" : "ITGTIME",
38     "Nskips" : "NDCMS",
39     "Ncols" : "NAXIS1",
40     "Nrows" : "NAXIS2",
41     "Npbin" : "NPBIN",
42     "Nsbin" : "NSBIN",
43     "ampl" : "AMPL",
44     "exposure_time" : "MEXP",
45     "read_time" : "MREAD"
46 }
47 },
48 "process":
49 {
50     "sequence": "RNvsNskipsPlot;CompressSkipperProcess;PedestalSubtractionProcess;
51     ChargeLossPlot;ClusterFinder;BuildClusterMask;FitDarkCurrentProcess",
52     "CompressSkipperProcess":
53     {
54         "func_to_compress" : ["mean","std"],
55         "save_image" : false
56     },
57     "PedestalSubtractionProcess":
58     {
59         "image" : "mean_compressed",
60         "method" : "gaussian_fit",
61         "__DEBUG__" : false,
62         "in_overscan" : false,
63         "use_mad" : false,
64         "axis" : "row",
65         "n_sigma_win_fit" : 3,
66         "n_sigma_to_mask" : 2,
67         "show_fit" : false,
```

```
67     "histequ" : false,
68     "save_image" : false
69 },
70 "CorrectElectronicColumnTransient":
71 {
72     "image" : "mean_compressed_pedestal_subtracted",
73     "col_start" : 1,
74     "col_end" : 10,
75     "subtract_median" : true,
76     "n_exp" : 1,
77     "fit_options" : "QSMER"
78 },
79 "CalibrationProcess":
80 {
81     "image" : "mean_compressed_pedestal_subtracted",
82     "gain" : {"U":5.0, "L":5.0}
83 },
84 "FitCalibrationConstant":
85 {
86     "image" : "mean_compressed_pedestal_subtracted",
87     "n_peaks" : 3,
88     "calibration" : {"U":10.0, "L":10.0},
89     "n_sigma_win_fit" : 3
90 },
91 "FitDarkCurrentProcess":
92 {
93     "image" : "mean_compressed_pedestal_subtracted",
94     "__DEBUG__" : false,
95     "__verbose__" : false,
96     "rows_to_mask" : {"L":[], "U":[]},
97     "cols_to_mask" : {"L":[], "U":[]},
98     "mask_clusters" : true,
99     "do_calibration" : true,
100     "calibration" : 10.8,
101     "n_peaks" : 5,
102     "binning_size" : 0.3,
103     "sigma_max" : {"L":3.0, "U":9.5},
104     "gain_min" : 2.0,
105     "gain_max" : {"L":17.0, "U":11.0},
106     "x_min" : -20,
107     "x_max" : 50
108 },
109 "FitDarkCurrentPerRow":
110 {
111     "image" : "mean_compressed_pedestal_subtracted",
112     "row_start" : 0,
113     "row_end" : 840,
```

```
114     "row_step" : 10,
115     "calibration" : 10.0,
116     "rows_to_mask" : {"L": [], "U": []},
117     "cols_to_mask" : {"L": [0,1], "U": [[638,639]]},
118     "n_peaks" : 3,
119     "binning_size" : 0.3,
120     "gain_min" : 8.0,
121     "gain_max" : 15.0,
122     "x_min" : -20,
123     "x_max" : 60
124 },
125 "FitDarkCurrentPerCol":
126 {
127     "image" : "mean_compressed_pedestal_subtracted",
128     "col_start" : 0,
129     "col_end" : -1,
130     "col_step" : 20,
131     "rows_to_mask" : {"L": [], "U": []},
132     "cols_to_mask" : {"L": [], "U": [[]]},
133     "calibration" : 10.0,
134     "n_peaks" : 5,
135     "binning_size" : 0.3,
136     "gain_min" : 8.0,
137     "gain_max" : 15.0,
138     "x_min" : -20,
139     "x_max" : 60
140 },
141 "ChargeLossPlot":
142 {
143     "skip_id_list" : [0,1,2,45],
144     "skip_id_baseline" : 52,
145     "histequ" : false,
146     "gray_palette" : false
147 },
148 "ChargeLossSkewnessProcess":
149 {
150     "use_overscan" : false,
151     "id_skip_reference" : 1,
152     "id_skip_start" : 2,
153     "id_skip_end" : -1,
154     "skip_step" : 20,
155     "kcl_threshold" : 3.2,
156     "kcl_n_sig" : 8,
157     "display" : true
158 },
159 "FFTNoisePlot":
160 {
```

```
161     },
162     "RNvsNskipsPlot":
163     {
164         "n_skips_per_block" :30,
165         "is_blank" : false
166     },
167     "ClusterFinder":
168     {
169         "spr_threshold" : {"U": [null,3,10], "L": [null,3,10]},
170         "spr_image" : "mean_compressed_pedestal_subtracted",
171         "spr_mask" : false,
172         "method" : 0,
173         "max_nearest_neighbor" : 1
174     },
175     "BuildClusterMask":
176     {
177         "cluster_size_min" : 1,
178         "N_col_pre" : 3,
179         "N_col_post" : 5,
180         "N_row_pre" : 1,
181         "N_row_post" : 1,
182         "cluster_E_min" : 10
183     },
184     "ApplySelectionCuts":
185     {
186         "cols" : [10,141,42,143,144,145,146,147,148,149,150],
187         "rows" : [1,2,3,149,150]
188     },
189     "GaussianFitProcess":
190     {
191         "image" : "mean_compressed_pedestal_subtracted",
192         "skip_rows" : [],
193         "in_trim_mean" : true,
194         "n_sigma" : 10
195     }
196 }
197 }
```

Appendix B

CCD configuration file

The configuration file contains a collection of settings and parameters that define the operational behaviour of the CCD and that can be varied to conduct different types of studies, such as the ones from this project. Additionally, the configuration file includes a sequencer that coordinates the clocks to control the transfer of charge through the CCD according to the parameters defined in the configuration file.

Example of a CCD configuration file:

```
1 [ccd]
2 sequencer_loc = /home/centos/DAMIC/CCDDrone_LBC/CCDSequencer-SkipperASM/
   firmware_pit_super_sequencer_UW2.lod
3
4 super_sequencer = true ; This is true only if the universal sequencer is being used
5 second_stage = UW2 ; Whether you are using the pinouts from UW v1 (older CCDs) or v2 (
   newer CCDs)
6
7 type = SK ; Possible types: DES and SK
8 columns = 650
9 rows = 100
10 NDCM = 3000 ; Number of skipper measurements.
11 RG_inv = false
12
13 AmplifierDirection = UL ; Possible values: U, L, UL.
14 HClkDirection = UL ; Possible values: U, L, UL.
15 VClkDirection = 1 ; Possible values: 1, 2.
16
17 Gain = 1 ; Gain can be only 1,2,5 or 10
18 ParallelBin = 1 ; Binning of the parallel clocks in the vertical direction.
19 SerialBin = 10 ; Binning of the serial clocks in the horizontal direction.
20
21 [timing]
22 ;Units: microseconds
23 IntegralTime = 12. ; Integration time
24 PedestalIntgWait = 2.5 ; Wait time before pedestal integration begins.
25 SignalIntgWait = 2.5 ; Wait time before signal integration begins.
26 DGWidth = 0.24 ; Width of the dump gate
27 OGWidth = 0.24 ; Width of OG to transfer charge from the SN to the SW or the other way
   around
28 RGWidth = 0.24 ; Width of RG in a skipping sequence.
29 SWPulseWidth = 0.24 ; Width of the SW pulse to push charge into the SN.
30
31 ;Charge, which is located at L, starts being clocked from the right to the left as
```

```
    follows:
32 ; 1. H-L-H
33 ; 2. L-L-H
34 ; 3. L-H-H
35 ; where H refers to the high values and L to the low values of the horizontal and
    vertical clocks potentials. This procedure continues so on and so forth. The
    timing of step 1 and 3 where only a single clock is low is controlled by VWidth
    and HWidth. The timing of step 2 where two clocks are low is controlled by
    VOverlapWidth and HOverlapWidth.
36
37 VWidth = 30. ; Width of the V-clocks when not overlapping.
38 VOverlapWidth = 20. ; Width of the V-clocks when two gates overlap.
39 HWidth = 1.25 ; Width of the H-clocks when not overlapping.
40 HOverlapWidth = 1.25 ; Width of the H-clocks when two gates overlap.
41
42 [clocks]
43 ;Units: volts
44 ;Common clocks for the SR1 and SR2: charge movement in the serial register
45 u_hclock_hi = 2. ; High voltage value of horizontal clocks clocking charge towards
    the U amplifier
46 u_hclock_lo = -0.5 ; Low voltage value of horizontal clocks clocking charge towards
    the U amplifier
47 l_hclock_hi = 2 ; High voltage value of horizontal clocks clocking charge towards the
    L amplifier
48 l_hclock_lo = -0.5 ; Low voltage value of horizontal clocks clocking charge towards
    the L amplifier
49
50 ;The following clocks are divided into SR1 clocks and SR2 clocks
51
52 ;The vertical clocks 1 move charge towards the serial register 1 (SR 1)
53 one_vclock_hi = 4.5. ; High voltage value of vertical clocks
54 one_vclock_lo = 1.5. ; Low voltage value of vertical clocks
55 ;The transfer gate 1 connects vertical clocks from the active region with horizontal
    clocks from the serial register 1 (SR1)
56 one_tg_hi = 4.0 ; High voltage value of the transfer gate
57 one_tg_lo = 1.5 ; Low voltage value of the transfer gate
58
59 one_dg_hi = -4. ; High voltage value of the dump gate.
60 one_dg_lo = -8. ; Low voltage value of the dump gate.
61 one_rg_hi = 5. ; High voltage value of the reset gate.
62 one_rg_lo = 3. ; Low voltage value of the reset gate
63
64 one_sw_hi = -3. ; High voltage value of the summing well
65 one_sw_lo = -10. ; Low voltage value of the summing well
66 one_og_hi = -4. ; High voltage value of the output gate
67 one_og_lo = -9. ; Low voltage value of the output gate
68
```

```
69 ;The vertical clocks 2 move charge towards the serial register 2 (SR 2)
70 two_vclock_hi = 4.5. ; High voltage value of vertical clocks
71 two_vclock_lo = 1.5. ; Low voltage value of vertical clocks
72 ;The transfer gate 2 connects vertical clocks from the active region with horizontal
    clocks from the serial register 2 (SR2)
73 two_tg_hi = 4.0 ; High voltage value of the transfer gate
74 two_tg_lo = 1.5 ; Low voltage value of the transfer gate
75
76 two_dg_hi = -4. ; High voltage value of the dump gate.
77 two_dg_lo = -8. ; Low voltage value of the dump gate.
78 two_rg_hi = 5. ; High voltage value of the reset gate.
79 two_rg_lo = 3. ; Low voltage value of the reset gate
80
81 two_sw_hi = -3. ; High voltage value of the summing well
82 two_sw_lo = -10. ; Low voltage value of the summing well
83 two_og_hi = -4. ; High voltage value of the output gate
84 two_og_lo = -9. ; Low voltage value of the output gate
85
86 [bias]
87 vsub = 60. ; Bias voltage [V]
88 ramp_down_rate = 15. ; Voltage rate that determines the duration of the voltage ramp
    down [V/s]
89 ramp_up_rate = 15. ; Voltage rate that determines the duration of the voltage ramp up
    [V/s]
90 hold_vsuboff_seconds = 9. ; Time to hold the potential at the lowest value [s]
91 turnoff_clock_voltage = 45. ; Voltage at which the clocks are turned off during the
    ramp down [V]
92 restart_clock_voltage = 20. ; Voltage at which the clocks are restarted during the
    ramp up [V]
93
94 ;Vdd voltages
95 vdd_1 = -19.
96 vdd_2 = -19.
97 ;Vref voltages
98 vref_1 = -7.0
99 vref_2 = -7.0
100 ;Vdrain voltages
101 drain_1 = -22.
102 drain_2 = -22.
103
104 opg_1 = 2.21 ; OpG is useful for DES only, but is still set regardless. The pins are
    distinct to DES CCDs.
105 opg_2 = 2.21 ; OpG is useful for DES only, but is still set regardless. The pins are
    distinct to DES CCDs.
106
107 battrelay = 10 ; Controls relay for battery box
108 video_offsets_U = 1000 ; Pedestal offset controls - U amplifier. Range: 0-4095
```

109 | video_offsets_L = 1000 ; Pedestal offset controls - L amplifier. Range: 0-4095 |

Appendix C

Guide to skipper CCD Start-Up and data-taking with the LEACH DAQ system: CCDDrone

C.1 CCD Start-Up

The detector operation begins by switching the LEACH controller (CCD controller) on. Then, the “bias board” power suppliers, the substrate voltage power supply and the amplifier board power supply are turned on. V_{dd} , V_R and V_{drain} are supplied by -19.00 V, -7.00 V and -22.00 V respectively. Through the [Slow Control System](#) the amplifier +/- board voltages, the power output controlled by AVC and the ramprate and setpoint temperature of the CTC 100 heater can be set. The amplifier board voltages +/- are supplied with +5 V and -5 V. The current on the amplifier board should be stable around ~ 0.140 A. The power output controlled by AVC is at 120.000 W, the ramprate heater is set at 0.016 K/s and the setpoint temperature is usually at 120.000 K.

The startup process for the CCD can be initiated through the DAQ computer (centos@gaepc6.ifca.unican.es). After logging in, it is recommended to create a separate screen session. This allows the terminal to continue running in the background, ensuring that the process persists even if the SSH connection to the computer is lost. In `gaepc6.ifca.unican.es` the CCDDrone directory is located in the home space called `~/DAMIC/CCDDrone_LBC/`. Within this folder the remaining steps should take place. To establish communication between the LEACH and CCD, i.e. to startup the CCD, the following command needs to be executed:

```
./CCDDStartup < path_to_config_folder > / < file_name.ini >
```

where `< path_to_config_folder >` needs to be replaced with the actual path to the configuration folder and `< file_name.ini >` with the appropriate name of the CCD configuration file. This procedure ensures that the CCD is properly initialized and ready for data acquisition. It restarts the LEACH controller, establishes connections to the LEACH and brings up the voltages on the CCD.

CCD Start-Up sets the beginning of the detector operation. Afterwards, CCD parameters need to be first set in the configuration file before starting the data-taking process (see [C.2](#)).

From time to time an erase procedure can be done to remove any accumulated extra charge on the CCD’s surface. The following command needs to be executed to perform this procedure:

```
./CCDDPerformEraseProcedure < path_to_config_folder > / < file_name.ini >
```

where `< path_to_config_folder >` needs to be replaced with the actual path to the configuration folder

and $\langle file_name.ini \rangle$ with the appropriate name of the CCD configuration file. This procedure erases surface charge (by applying a V_{sub} -cycle) and sets the CCD in IDLE mode, i.e. nominal clocks and bias voltages are applied so that the CCD clocks charge according to the directions specified in the configuration file. During the IDLE mode, the selected amplifier(s) perform the readout but pixel values are not store, i.e. no data is acquired during the IDLE mode. The erase procedure produces undesired patterns of charge in the images, so it is important to take a few “cleaning images” to remove these patterns. The different stages of the erase procedure are represented in the sketch from Figure C.1.

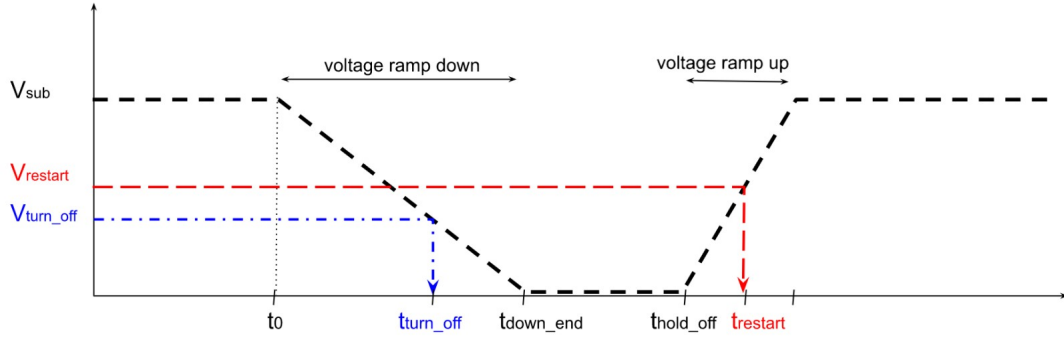


Figure C.1: Scheme of the CCDPerformAndErase procedure. V_{sub} [V] is the bias voltage applied during the procedure, $ramp_down_rate$ [V/s] is the voltage rate that determines the duration of the voltage ramp down, $ramp_up_rate$ [V/s] is the voltage rate that determines the duration of the voltage ramp up, $hold_vsuboff_seconds$ [s] is the time to hold the potential at the lowest value, $turnoff_clock_voltage$ [V] is the voltage at which the clocks are turned off during the ramp down and $restart_clock_voltage$ [V] is the voltage at which the clocks are restarted during the ramp up. These parameters are set to 45 / 60 V, 15 V/s, 15 V/s, 9 s, 45 V and 20 V respectively.

C.2 Data-taking process

The data taking process involves a series of steps that are shown below:

1. Applying new operating settings: To configure the CCD with the desired settings specified in the CCD configuration file, the following command needs to be used:

```
./CCDDApplyNewSettings < path_to_config_folder > / < file_name.ini >
```

where $\langle path_to_config_folder \rangle$ needs to be replaced with the actual path to the configuration folder and $\langle file_name.ini \rangle$ with the appropriate name of the configuration file.

2. Initiating the CCD exposure: CCD time exposure starts by executing the following command:

```
./CCDDExpose X < path_to_config_folder > / < file_name.ini >
```

where X represents the duration in seconds for which the CCD will be exposed, $\langle path_to_config_folder \rangle$ needs to be replaced with the desired folder path where the image will be stored and $\langle file_name.ini \rangle$ with the appropriate name for the image fits file. During the exposure time clocks are set to the accumulation phase.

3. Reading out the charge: At the end of the exposure, the charge is read out using the selected amplifier(s).

C.2.1 Scripts

The previously described data-taking process can be used for taking images one by one. Multiple images can be programmed to be taken using scripts. These scripts have been constantly modified depending on the desired changes in the CCD configuration parameters, the number of images wanted to be taken, and, in the case of skip images, the addition of the “cleaning procedure” between skip images.

Example of a script:

```

1 #!/bin/bash
2
3 # Definition of the output folder (DAYFOLDER) based on the current date using the date
  command
4 DAYFOLDER=$(date +"%Y%m%d")
5
6 # Creation of the output folder using the mkdir -p command, ensuring that the
  directory is created if it does not exist
7 mkdir -p /mnt/1ABAA95DBAA93663/Users/Public/DATA/pruebas_maria/${DAYFOLDER}
8
9 # The variable DATADIR is set as the path to the data directory within the output
  folder
10 DATADIR=/mnt/1ABAA95DBAA93663/Users/Public/DATA/pruebas_maria/${DAYFOLDER}
11
12 # Exposure time of the CCD
13 EXPOSURE=2
14
15 # This variable can be defined as 1 or 2 depending on the type of images wanted to be
  taken
16 CONDITION=1
17
18 # To take successive skipper images for different values of integration time
19 if [ "$CONDITION" = "1" ];
20 then
21   # Loop over integration time values
22   for it in 5 7 9 11 13 15 17 19 21 23 25
23   do
24     # To generate the configuration file with specific settings and parameters defined
      in the create_settings_for_ccddrone file along with changes to the
      corresponding parameters defined after -s
25     create_settings_for_ccddrone -o /mnt/1ABAA95DBAA93663/Users/Public/DATA/config/
      config_${DAYFOLDER}_OPT${CONDITION}_ittime.ini -s cols:650 rows:100 skips:1500
      vbin:10 hbin:1 ittime:${it} hwidth:1.25 hlapwidth:1.25 hhi_u:2.0 hhi_l:2.0
      vsub:60.0 swlo_2:-10.0 swlo_1:-10.0 vdir:1 vlapwidth:20
26
27     # To generate the configuration file for cleaning images
28     create_settings_for_ccddrone -o /mnt/1ABAA95DBAA93663/Users/Public/DATA/config/
      config_${DAYFOLDER}_clean.ini -s cols:325 rows:85 skips:1 vbin:20 hbin:20
      ittime:5.0 hwidth:1.25 hlapwidth:1.25 hhi_u:3.0 hhi_l:3.0 vsub:60.0

```

```

29
30 # Clean the CCD several times ("cleaning procedure") before taking skipper images
31 for c in `seq 1 5`
32 do
33     echo "Clean image: ${c}"
34     # Apply settings for the cleaning image
35     ./CCDDApplyNewSettings /mnt/1ABAA95DBAA93663/Users/Public/DATA/config/config_${
        DAYFOLDER}_clean.ini
36     sleep 10
37     # Expose and read the image
38     ./CCDDExpose ${EXPOSURE} ${DATADIR}/"ironman_${DAYFOLDER}_OPT${CONDITION}
        _60V_it12_325x85_bin20x20_saturation_study_it${it}_${c}_clean4.fits"
39     sleep 5
40 done
41
42 # Skipper image
43 echo "Integration time: ${it}"
44 # Apply settings for the skipper image
45 ./CCDDApplyNewSettings /mnt/1ABAA95DBAA93663/Users/Public/DATA/config/config_${
        DAYFOLDER}_OPT${CONDITION}_ittime.ini
46 sleep 10
47 # Expose and read the image
48 ./CCDDExpose ${EXPOSURE} ${DATADIR}/"ironman_${DAYFOLDER}_OPT${CONDITION}
        _UL1_60V_650x100_bin10x1_1500skips_5FastCleaning_it${it}_hhi2.fits"
49 sleep 10
50 done
51
52
53 # To take successive skipper images with the same configuration parameters
54 elif [ "$CONDITION" = "2" ];
55 then
56     # To generate the configuration file with specific settings and parameters defined
        in the create_settings_for_ccddrone file along with changes to the
        corresponding parameters defined after -s
57     create_settings_for_ccddrone -o config/config_${DAYFOLDER}_OPT${CONDITION}.ini -s
        cols:650 rows:100 skips:1500 vbin:10 hbin:1 ittime:12.0 hwidth:1.25 hlapwidth
        :1.25 hhi_u:2.0 hhi_l:2.0 vsub:60.0 swlo_2:-10.0 swlo_1:-10.0 vdir:1 vlapwidth
        :20.0
58
59     # To generate the configuration file for cleaning images
60     create_settings_for_ccddrone -o config/config_${DAYFOLDER}_clean.ini -s cols:325
        rows:85 skips:1 vbin:20 hbin:20 ittime:5.0 hwidth:1.25 hlapwidth:1.25 hhi_u
        :3.0 hhi_l:3.0 vsub:60.0 vdir:1
61
62     # With this loop, the desired number of skipped images are taken with the
        previously defined configuration parameters and settings and doing a "cleaning
        procedure" between each one of them.

```

```
63  for i in `seq 1 5`
64  do
65      # Clean the CCD several times before taking skipper images
66      for c in `seq 1 5`
67      do
68          echo "Clean image: ${i},${c}"
69          # Apply settings for the cleaning image
70          ./CCDDApplyNewSettings config/config-${DAYFOLDER}_clean.ini
71          sleep 10
72          # Expose and read the image
73          ./CCDDEExpose ${EXPOSURE} ${DATADIR}/"ironman-${DAYFOLDER}_OPT${CONDITION}
              _60V_it12_325x85_bin20x20_saturation_study_${i}-${c}_clean.fits"
74          sleep 5
75      done
76
77      # Skipper image
78      echo "Skipper Image: ${i}"
79      # Apply settings for the skipper image
80      ./CCDDApplyNewSettings config/config-${DAYFOLDER}_OPT${CONDITION}.ini
81      sleep 10
82      # Expose and read the image
83      ./CCDDEExpose ${EXPOSURE} ${DATADIR}/"ironman-${DAYFOLDER}_OPT${CONDITION}
              _UL1_60V_it12_650x100_bin10x1_1500skips_5FastCleaning_${i}.fits"
84      sleep 10
85  done
86
87  fi
```

Appendix D

Python codes

D.1 Integration time

The provided python code generates plots of the pixel readout noise as a function of the integration time for skip images. The input data must be modified based on the specific values of integration time (μs), the pixel readout noise σ (ADUs) and gain k (ADUs per electron). These last magnitudes are provided by dark current fit plots.

```
1
2 # Import necessary libraries
3 import numpy as np
4 import matplotlib.pyplot as plt
5
6 # Input data
7 integrationtime = [5, 7, 8, 9, 11, 13, 15, 17, 19, 21, 23, 25]
8 k_values = [4.40, 6.09, 7.19, 8.123, 9.757, 11.44, 13.38, 15.47, 17.32, 18.8, 20.35,
9             22.91]
10 delta_k_values = [0.13, 0.17, 0.07, 0.123, 0.131, 0.12, 0.15, 0.18, 0.19, 0.2, 0.23,
11                  0.25]
12 sigma_values = [1.053, 1.402, 1.251, 1.263, 1.392, 1.579, 1.737, 1.994, 2.217, 2.40,
13                 2.566, 2.989]
14 delta_sigma_values = [0.004, 0.006, 0.005, 0.005, 0.006, 0.006, 0.007, 0.008, 0.009,
15                       0.01, 0.011, 0.012]
16
17 # Empty lists to store the pixel readout noise and its error in units of electrons
18 e_values = []
19 propagated_errors = []
20
21 # Function to calculate the pixel readout noise in units of electrons and its error by
22 # propagation of errors
23 def calculate_e_and_propagated_error(sigma, k, delta_sigma, delta_k):
24     """
25     Calculate the propagated error for the pixel readout noise.
26
27     Args:
28         sigma (float): Pixel readout noise in units of ADUs.
29         k (float): Gain (ADUs per e-).
30         delta_sigma (float): Uncertainty in the sigma value.
31         delta_k (float): Uncertainty in the k value.
```

```

28     Returns:
29         Tuple containing the pixel readout noise in units of e- and its propagated
           error.
30     """
31     e = sigma / k
32     error = np.sqrt((delta_sigma / k)**2 + (sigma * delta_k / k**2)**2)
33     return e, error
34
35 # Iterate over the input data and calculate propagated error
36 for i in range(len(sigma_values)):
37     e, error = calculate_e_and_propagated_error(sigma_values[i], k_values[i],
           delta_sigma_values[i], delta_k_values[i])
38     e_values.append(e)
39     propagated_errors.append(error)
40
41 # Plot the data
42 plt.plot(integrationtime, e_values, 'o', c='b', markersize=3, label="1500 skips
           daytime images 14/06/2023")
43 plt.errorbar(integrationtime, e_values, yerr=propagated_errors, fmt='none', ecolor='b'
           , capsize=3)
44 plt.grid(True)
45 plt.xlabel(r'Integration Time ( $\mu$ s)')
46 plt.ylabel('Read Noise (e-)')
47 plt.legend()
48
49 # Save the plot to a file
50 plt.savefig("integrationtime_20230614_afternoon.png")
51
52 # Display the plot
53 plt.show()

```

D.2 Average FITS image

The provided Python code generates an average FITS image by combining 50 FITS images that were reprocessed using the analysis software WADERS (see A.2). This given python code has been modified depending on the average image wanted. In the following example, it is shown the code for obtaining the average image at 200 K, as the 50 input images correspond to images taken at this temperature value.

```

1
2 # Import necessary libraries
3 from astropy.io import fits
4 import numpy as np
5
6 # Load the FITS images
7 # Open each FITS file and assign it to a variable
8 hdul1 = fits.open('ironman_20230531_OPT3_60V_UL2_it12_6500x1700_5FastCleaning
9 Images_temp200_1_60exp_waders.fits')

```

```
10 hdul2 = fits.open('ironman_20230531_OPT3_60V_UL2_it12_6500x1700_5FastCleaning
11 Images_temp200_2_60exp_waders.fits')
12 hdul3 = fits.open('ironman_20230531_OPT3_60V_UL2_it12_6500x1700_5FastCleaning
13 Images_temp200_3_60exp_waders.fits')
14 hdul4 = fits.open('ironman_20230531_OPT3_60V_UL2_it12_6500x1700_5FastCleaning
15 Images_temp200_4_60exp_waders.fits')
16 hdul5 = fits.open('ironman_20230531_OPT3_60V_UL2_it12_6500x1700_5FastCleaning
17 Images_temp200_5_60exp_waders.fits')
18 hdul6 = fits.open('ironman_20230531_OPT3_60V_UL2_it12_6500x1700_5FastCleaning
19 Images_temp200_6_60exp_waders.fits')
20 hdul7 = fits.open('ironman_20230531_OPT3_60V_UL2_it12_6500x1700_5FastCleaning
21 Images_temp200_7_60exp_waders.fits')
22 hdul8 = fits.open('ironman_20230531_OPT3_60V_UL2_it12_6500x1700_5FastCleaning
23 Images_temp200_8_60exp_waders.fits')
24 hdul9 = fits.open('ironman_20230531_OPT3_60V_UL2_it12_6500x1700_5FastCleaning
25 Images_temp200_9_60exp_waders.fits')
26 hdul10 = fits.open('ironman_20230531_OPT3_60V_UL2_it12_6500x1700_5FastCleaning
27 Images_temp200_10_60exp_waders.fits')
28 hdul11 = fits.open('ironman_20230531_OPT3_60V_UL2_it12_6500x1700_5FastCleaning
29 Images_temp200_11_60exp_waders.fits')
30 hdul12 = fits.open('ironman_20230531_OPT3_60V_UL2_it12_6500x1700_5FastCleaning
31 Images_temp200_12_60exp_waders.fits')
32 hdul13 = fits.open('ironman_20230531_OPT3_60V_UL2_it12_6500x1700_5FastCleaning
33 Images_temp200_13_60exp_waders.fits')
34 hdul14 = fits.open('ironman_20230531_OPT3_60V_UL2_it12_6500x1700_5FastCleaning
35 Images_temp200_14_60exp_waders.fits')
36 hdul15 = fits.open('ironman_20230531_OPT3_60V_UL2_it12_6500x1700_5FastCleaning
37 Images_temp200_15_60exp_waders.fits')
38 hdul16 = fits.open('ironman_20230531_OPT3_60V_UL2_it12_6500x1700_5FastCleaning
39 Images_temp200_16_60exp_waders.fits')
40 hdul17 = fits.open('ironman_20230531_OPT3_60V_UL2_it12_6500x1700_5FastCleaning
41 Images_temp200_17_60exp_waders.fits')
42 hdul18 = fits.open('ironman_20230531_OPT3_60V_UL2_it12_6500x1700_5FastCleaning
43 Images_temp200_18_60exp_waders.fits')
44 hdul19 = fits.open('ironman_20230531_OPT3_60V_UL2_it12_6500x1700_5FastCleaning
45 Images_temp200_19_60exp_waders.fits')
46 hdul20 = fits.open('ironman_20230531_OPT3_60V_UL2_it12_6500x1700_5FastCleaning
47 Images_temp200_20_60exp_waders.fits')
48 hdul21 = fits.open('ironman_20230531_OPT3_60V_UL2_it12_6500x1700_5FastCleaning
49 Images_temp200_21_60exp_waders.fits')
50 hdul22 = fits.open('ironman_20230531_OPT3_60V_UL2_it12_6500x1700_5FastCleaning
51 Images_temp200_22_60exp_waders.fits')
52 hdul23 = fits.open('ironman_20230531_OPT3_60V_UL2_it12_6500x1700_5FastCleaning
53 Images_temp200_23_60exp_waders.fits')
54 hdul24 = fits.open('ironman_20230531_OPT3_60V_UL2_it12_6500x1700_5FastCleaning
55 Images_temp200_24_60exp_waders.fits')
56 hdul25 = fits.open('ironman_20230531_OPT3_60V_UL2_it12_6500x1700_5FastCleaning
```

```
57 Images_temp200_25_60exp_waders.fits')
58 hdul26 = fits.open('ironman_20230531_OPT3_60V_UL2_it12_6500x1700_5FastCleaning
59 Images_temp200_26_60exp_waders.fits')
60 hdul27 = fits.open('ironman_20230531_OPT3_60V_UL2_it12_6500x1700_5FastCleaning
61 Images_temp200_27_60exp_waders.fits')
62 hdul28 = fits.open('ironman_20230531_OPT3_60V_UL2_it12_6500x1700_5FastCleaning
63 Images_temp200_28_60exp_waders.fits')
64 hdul29 = fits.open('ironman_20230531_OPT3_60V_UL2_it12_6500x1700_5FastCleaning
65 Images_temp200_29_60exp_waders.fits')
66 hdul30 = fits.open('ironman_20230531_OPT3_60V_UL2_it12_6500x1700_5FastCleaning
67 Images_temp200_30_60exp_waders.fits')
68 hdul31 = fits.open('ironman_20230531_OPT3_60V_UL2_it12_6500x1700_5FastCleaning
69 Images_temp200_31_60exp_waders.fits')
70 hdul32 = fits.open('ironman_20230531_OPT3_60V_UL2_it12_6500x1700_5FastCleaning
71 Images_temp200_32_60exp_waders.fits')
72 hdul33 = fits.open('ironman_20230531_OPT3_60V_UL2_it12_6500x1700_5FastCleaning
73 Images_temp200_33_60exp_waders.fits')
74 hdul34 = fits.open('ironman_20230531_OPT3_60V_UL2_it12_6500x1700_5FastCleaning
75 Images_temp200_34_60exp_waders.fits')
76 hdul35 = fits.open('ironman_20230531_OPT3_60V_UL2_it12_6500x1700_5FastCleaning
77 Images_temp200_35_60exp_waders.fits')
78 hdul36 = fits.open('ironman_20230531_OPT3_60V_UL2_it12_6500x1700_5FastCleaning
79 Images_temp200_36_60exp_waders.fits')
80 hdul37 = fits.open('ironman_20230531_OPT3_60V_UL2_it12_6500x1700_5FastCleaning
81 Images_temp200_37_60exp_waders.fits')
82 hdul38 = fits.open('ironman_20230531_OPT3_60V_UL2_it12_6500x1700_5FastCleaning
83 Images_temp200_38_60exp_waders.fits')
84 hdul39 = fits.open('ironman_20230531_OPT3_60V_UL2_it12_6500x1700_5FastCleaning
85 Images_temp200_39_60exp_waders.fits')
86 hdul40 = fits.open('ironman_20230531_OPT3_60V_UL2_it12_6500x1700_5FastCleaning
87 Images_temp200_40_60exp_waders.fits')
88 hdul41 = fits.open('ironman_20230531_OPT3_60V_UL2_it12_6500x1700_5FastCleaning
89 Images_temp200_41_60exp_waders.fits')
90 hdul42 = fits.open('ironman_20230531_OPT3_60V_UL2_it12_6500x1700_5FastCleaning
91 Images_temp200_42_60exp_waders.fits')
92 hdul43 = fits.open('ironman_20230531_OPT3_60V_UL2_it12_6500x1700_5FastCleaning
93 Images_temp200_43_60exp_waders.fits')
94 hdul44 = fits.open('ironman_20230531_OPT3_60V_UL2_it12_6500x1700_5FastCleaning
95 Images_temp200_44_60exp_waders.fits')
96 hdul45 = fits.open('ironman_20230531_OPT3_60V_UL2_it12_6500x1700_5FastCleaning
97 Images_temp200_45_60exp_waders.fits')
98 hdul46 = fits.open('ironman_20230531_OPT3_60V_UL2_it12_6500x1700_5FastCleaning
99 Images_temp200_46_60exp_waders.fits')
100 hdul47 = fits.open('ironman_20230531_OPT3_60V_UL2_it12_6500x1700_5FastCleaning
101 Images_temp200_47_60exp_waders.fits')
102 hdul48 = fits.open('ironman_20230531_OPT3_60V_UL2_it12_6500x1700_5FastCleaning
103 Images_temp200_48_60exp_waders.fits')
```

```
104 hdul49 = fits.open('ironman_20230531_OPT3_60V_UL2_it12_6500x1700_5FastCleaning
105 Images_temp200_49_60exp_waders.fits')
106 hdul50 = fits.open('ironman_20230531_OPT3_60V_UL2_it12_6500x1700_5FastCleaning
107 Images_temp200_50_60exp_waders.fits')
108
109 """
110 The image data needs to be extracted from the first HDU of each FITS file. HDU stands
    for Header Data Unit, which is a self contained unit of data within a FITS file.
    Each HDU consists of a header and data section. In the case of an image HDU, the
    data section contains a two-dimensional array of pixel values representing the
    image. The data section can be accessed using the data attribute of an HDU object,
    e.g., hdul1[0].data
111 """
112 data1 = hdul1[0].data
113 data2 = hdul2[0].data
114 data3 = hdul3[0].data
115 data4 = hdul4[0].data
116 data5 = hdul5[0].data
117 data6 = hdul6[0].data
118 data7 = hdul7[0].data
119 data8 = hdul8[0].data
120 data9 = hdul9[0].data
121 data10 = hdul10[0].data
122 data11 = hdul11[0].data
123 data12 = hdul12[0].data
124 data13 = hdul13[0].data
125 data14 = hdul14[0].data
126 data15 = hdul15[0].data
127 data16 = hdul16[0].data
128 data17 = hdul17[0].data
129 data18 = hdul18[0].data
130 data19 = hdul19[0].data
131 data20 = hdul20[0].data
132 data21 = hdul21[0].data
133 data22 = hdul22[0].data
134 data23 = hdul23[0].data
135 data24 = hdul24[0].data
136 data25 = hdul25[0].data
137 data26 = hdul26[0].data
138 data27 = hdul27[0].data
139 data28 = hdul28[0].data
140 data29 = hdul29[0].data
141 data30 = hdul30[0].data
142 data31 = hdul31[0].data
143 data32 = hdul32[0].data
144 data33 = hdul33[0].data
145 data34 = hdul34[0].data
```

```
146 data35 = hdul35[0].data
147 data36 = hdul36[0].data
148 data37 = hdul37[0].data
149 data38 = hdul38[0].data
150 data39 = hdul39[0].data
151 data40 = hdul40[0].data
152 data41 = hdul41[0].data
153 data42 = hdul42[0].data
154 data43 = hdul43[0].data
155 data44 = hdul44[0].data
156 data45 = hdul45[0].data
157 data46 = hdul46[0].data
158 data47 = hdul47[0].data
159 data48 = hdul48[0].data
160 data49 = hdul49[0].data
161 data50 = hdul50[0].data
162
163 # List of all the data variables
164 data_list = [data1, data2, data3, data4, data5, data6, data7, data8, data9, data10,
              data11, data12, data13, data14, data15, data16, data17, data18, data19, data20,
              data21, data22, data23, data24, data25, data26, data27, data28, data29, data30,
              data31, data32, data33, data34, data35, data36, data37, data38, data39, data40,
              data41, data42, data43, data44, data45, data46, data47, data48, data49, data50]
165
166 # Sum up all the data variables in the list
167 total_sum = sum(data_list)
168
169 # Divide the total sum by the number of data variables
170 mean = total_sum / len(data_list)
171
172
173 # Create a new FITS HDU with the mean data
174 mean_hdu = fits.PrimaryHDU(mean)
175
176 # Write the mean HDU to a new FITS file
177 mean_hdu.writeto('average_image200.fits', overwrite=True)
```